EHD2-mediated restriction of caveolar dynamics regulates cellular lipid uptake

Claudia Matthäus[1,9*], Ines Lahmann[2,9], Séverine Kunz[3], Wenke Jonas[4], Arthur Alves Melo[1], Martin Lehmann[5], Elin Larsson[6], Richard Lundmark[6,10], Volker Haucke[5,10], Dominik N. Müller[7,10], Annette Schürmann[4,10], Carmen Birchmeier[2,10], Oliver Daumke[1,8,10,11*]

[1] Crystallography, Max-Delbrück-Center for Molecular Medicine, Berlin, Germany

[2] Signal Transduction/Developmental Biology, Max-Delbrück-Center for Molecular Medicine, Berlin, Germany

[3] Electron Microscopy Facility, Max-Delbrück-Center for Molecular Medicine, Berlin, Germany

[4] Experimental Diabetology, German Institute of Human Nutrition, German Center for Diabetes Research, München-Neuherberg, Potsdam, Germany

[5] Dept. of Molecular Pharmacology & Cell Biology and Imaging Core Facility, Leibniz-Forschungsinstitut für Molekulare Pharmakologie, Berlin, Germany

[6] Integrative Medical Biology, Umeå University, 901 87 Umeå, Sweden

[7] Experimental & Clinical Research Center, a cooperation between Charité Universitätsmedizin Berlin and Max Delbrück Center for Molecular Medicine, Berlin, Germany

[8] Institute of Chemistry and Biochemistry, Freie Universität Berlin, Takustrasse 6, 14195 Berlin, Germany
Lead contact

[9] These authors contributed equally

[10] Senior author

[11] Lead contact

*Corresponding authors

Correspondence: claudia.matthaeus@mdc-berlin.de; oliver.daumke@mdc-berlin.de

Abstract

Eps15-homology domain containing protein 2 (EHD2) is a dynamin-related ATPase located at the neck of caveolae, but its physiological function has remained unclear. We found that global genetic ablation of EHD2 in mice led to increased fat deposits in several organs. This organismic phenotype was paralleled at the cellular level by an increased lipid uptake via a CD36-dependent pathway, an elevated number of detached caveolae and higher caveolar mobility. Following a high fat diet, various enzymes involved in *de novo* fatty acid synthesis were down-regulated in EHD2 KO mice. Furthermore, EHD2 expression itself was down-regulated in the visceral fat of two obese mouse models and in diet-induced obesity. Thus, EHD2 controls a cell-autonomous, caveolae-dependent lipid uptake pathway, implicating a role of EHD2 in fat accumulation and obesity.

Keywords: EHD proteins, caveolae, fatty acid uptake, CD36, lipid metabolism, obesity

Introduction

Caveolae are small membrane invaginations of the plasma membrane that are abundantly found in adipocytes, endothelial and muscle cells (Cheng and Nichols, 2016). They have been implicated in the regulation of membrane tension (Sinha *et al.*, 2011; Torrino *et al.*, 2018), in mediating lipid metabolism (Liu *et al.*, 2008), or in acting as distinct sites for specific and highly regulated signaling cascades such as the endothelial nitric oxide synthase (eNOS)-nitric oxide (NO) pathway (Ju *et al.*, 1997). The characteristically shaped caveolar bulb has a typical diameter of 50 - 100 nm and is connected to the cell surface via a narrow neck region. The integral membrane protein Caveolin (with three isoforms in human, Cav1-3) and the peripheral membrane protein Cavin (with four isoforms in human, Cavin1-4) build a mesh-like coat around the caveolar bulb (Ludwig *et al.*, 2013; Kovtun *et al.*, 2015; Mohan *et al.*, 2015; Ludwig, Nichols and Sandin, 2016; Stoeber *et al.*, 2016). In addition, BAR domain containing proteins of the PACSIN/syndapin family (PACSIN1-3 in human) participate in the biogenesis of caveolae (Hansen, Howard and Nichols, 2011; Senju *et al.*, 2011; Seemann *et al.*, 2017).

Loss of Cav1/Cav3 or Cavin1 results in a complete lack of caveolae from the plasma membrane (Drab *et al.*, 2001; Hill *et al.*, 2008; Liu *et al.*, 2008). Also, Cavin2 knockout (KO) mice show a decreased number of caveolae at the plasma membrane in adipocytes and lung endothelium, but not in cardiomyocytes or heart endothelium, suggesting a cell-type specific function (Hansen *et al.*, 2013). In contrast, loss of the muscle-enriched PACSIN3/syndapin III leads to the loss of caveolae in cardiomyocytes (Seemann *et al.*, 2017). The deletion of Cavin3 alone does not alter caveolae formation or caveolar protein assembly (Hansen *et al.*, 2013; Liu *et al.*, 2014).

Cav1 KO mice suffer from cardiomyopathy, pulmonary hypertension, endothelium-dependent relaxation problems and defective lipid metabolism (Cheng and Nichols, 2016). In agreement with the latter, Cav1 KO mice are resistant to high fat diet-induced obesity (Razani *et al.*, 2002) and display smaller white adipocytes and fat pads (Martin *et al.*, 2012). Furthermore, increased levels of triglycerides and fatty

72 acids are found in blood plasma samples obtained from Cav1 KO mice suggesting a reduced cellular uptake
73 of fatty acids (Razani *et al.*, 2002). A similar metabolic phenotype was found in mice lacking Cavin1 (Hill *et*
74 *al.*, 2008; Liu *et al.*, 2008; Ding *et al.*, 2014). Conversely, overexpression of Cav1 in adipocytes results in
75 enhanced fat accumulation, enlarged adipocytes and lipid droplets (LDs) (Briand *et al.*, 2014). An increased
76 number of caveolae is also found at the plasma membrane of Cav1 overexpressing adipocytes. These
77 results suggest that caveolae are involved in fat accumulation in adipocytes and may promote fatty acid
78 uptake (Pohl *et al.*, 2004). However, the molecular mechanisms of caveolae-dependent fat uptake have
79 remained obscure.

80 Eps15 homology domain containing protein 2 (EHD2) localizes to the caveolar neck region (Morén
81 *et al.*, 2012; Stoeber *et al.*, 2012; Ludwig *et al.*, 2013). The protein belongs to the dynamin-related EHD
82 ATPase family, which comprises four members in human (EHD1-4), and shows strong expression in human
83 adipose and muscle tissue (human protein atlas) (Uhlén *et al.*, 2015). EHD is built of an N-terminal GTPase
84 (G)-domain, which mediates dimerization and oligomerization, a helical domain containing the membrane
85 binding site, and a C-terminal regulatory Eps15 homology (EH)-domain. The proteins exist in a closed auto-
86 inhibited conformation in solution (Daumke *et al.*, 2007). When recruited to membranes, a series of
87 conformational changes aligns the phospholipid binding sites with the membrane and facilitates
88 oligomerization of EHD2 into ring-like structures (Shah *et al.*, 2014; Hoernke *et al.*, 2017; Melo *et al.*,
89 2017).

90 Down-regulation of EHD2 in cell culture results in decreased surface association and increased
91 mobility of caveolae, whereas EHD2 overexpression stabilizes caveolae at the plasma membrane (Morén
92 *et al.*, 2012; Stoeber *et al.*, 2012; Mohan *et al.*, 2015; Shvets *et al.*, 2015). This led to the hypothesis that
93 formation of an EHD2-ring at the neck of caveolae restricts caveolar mobility within the membrane. In
94 agreement with this hypothesis, EHD2 assembles in an ATP-dependent fashion into ring-like oligomers *in*
95 *vitro* and induces the formation of tubular liposomes with an inner diameter of 20 nm, corresponding to

96 the diameter of the caveolar neck (Daumke et al., 2007). Whether EHD2 also controls caveolar membrane
97 dynamics *in vivo* and what the physiological consequences of EHD2 loss at the organismic level are, is
98 unknown.

99 In this study, we found that EHD2 KO mice revealed enlarged fat accumulations in several organs,
100 and increased lipid droplets (LDs) in caveolae-harboring cell types like adipocytes, muscle or liver cells. In
101 tissue and cells lacking EHD2, caveolae were frequently detached from the plasma membrane and
102 displayed elevated mobility. We demonstrate that fatty acid uptake via the fatty acid translocase CD36 is
103 increased in adipocytes from EHD2 KO mice. Furthermore, in two obesity mouse models or after high fat
104 diet, reduced EHD2 expression and an increased numbers of detached caveolae were found in visceral fat.
105 Our data establish EHD2 as a negative regulator of caveolae-dependent lipid uptake and implicate a crucial
106 role of caveolar stability and dynamics for lipid homeostasis and obesity.
107
108 **Results**
109 **Generation of EHD2 knockout mouse model**
110 To elucidate the expression pattern of EHD2, immunostainings on cryostat sections of C57BL6/N
111 E15 mouse embryos were performed. They revealed strong EHD2 expression in the developing heart (Fig.
112 1A, see arrow), blood vessels (Fig. 1A, e.g. umbilical cord marked by star) and brown adipose tissue (BAT,
113 Fig. 1A, see arrow head), e.g. in tissues where caveolae are particularly abundant (Cheng and Nichols,
114 2016). These results were corroborated by *in situ* hybridizations against EHD2 mRNA, which indicated
115 strong EHD2 expression in BAT of an E18 C57BL6/N embryo (Fig. S1A). Intense EHD2 staining was also
116 observed in cryostat sections of adult C57BL6/N heart, white adipocyte tissue (WAT) and BAT (Fig. 1B-D).
117 To examine the physiological function of EHD2, a mouse strain with LoxP recognition sites
118 surrounding exon 3 and intron 3 of the *Ehd2* gene was engineered (Fig. 1E). Exon 3 encodes part of the
119 highly conserved GTPase domain (residues 137-167), and its deletion is predicted to result in non-

functional protein. Following global removal of exon 3 by crossings with a germ-line specific Cre-deleter strain, offspring mice were back-crossed with the C57BL6/N mouse strain for five generations, yielding a global EHD2 KO mouse model.

Genotyping of offspring confirmed the successful deletion of EHD2 exon 3 in EHD2 del/del animals (Fig. 1F) and real-time PCR revealed the absence of EHD2 mRNA in the EHD2 del/del tissue (Fig. 1G). Western blot analysis of EHD2 +/+ and del/+ tissues indicated the expression of EHD2 in several organs, such as heart, muscle, fat, lung, intestine and bladder, compared to its complete loss in EHD2 del/del mice (Fig. 1H). Cav1 and Cavin1 protein levels remained unchanged upon loss of EHD2. Immunostaining of cryostat sections obtained from EHD2 del/del brown adipose tissue did not reveal any significant differences in Cav1 or Cavin1 expression and localization (Fig. S1B). Furthermore, BAT immunostainings in adult mice illustrated the same high expression of EHD2 for +/+ and del/+ mice, whereas the EHD2 KO mice (del/del) showed a complete loss of EHD2 staining (Fig. 1I). In adult heart sections, specific staining of EHD2 in +/+ and del/+ mice was observed, and again no staining was seen in EHD2 KO mice (Fig. S1C).

Loss of EHD2 results in increased lipid accumulation

EHD2 del/del mice were born in normal Mendelian ratios, were fertile and did not show an obvious phenotype upon initial inspection. However, when one year-old EHD2 del/del male mice were dissected, the heart was surrounded by white fat deposits, and an increased amount of epigonadal and periinguinal white fat was observed, in contrast to the EHD2 del/+ male sibling controls or C57BL6/N male mice (Fig. 2A, C, Fig. S2A). Notably, heart and body weight did not differ in EHD2 del/del compared to EHD2 del/+ mice (Fig. 2B-D).

When analyzed in more detail, white adipocytes of EHD2 del/del mice showed an increased cell size compared to adipocytes of EHD2 del/+ mice (Fig. 2E, F), likely due to increased lipid storage. Indeed, lipid composition measurements of WAT indicated an increased amount of storage lipids (mainly

144 triacylglycerol) in EHD2 del/del mice compared to EHD2 del/+ (Fig. 2G). Similarly, elevated fat
145 accumulations in LDs were found in EHD2 del/del BAT (Fig. 2H). Histological inspections of BAT paraffin
146 and cryostat sections stained against the LD coat protein Perilipin1 indicated an increased LD size in EHD2
147 del/del BAT compared to EHD2 del/+ or C57BL6/N mice (Fig. 2I, J, Fig. S2B-D). Moreover, liver of EHD2
148 del/del mice displayed a yellowish appearance, suggesting increased fat accumulation (Fig. 2K). This was
149 confirmed by Oil red O staining of liver sections (Fig. 2L, Fig. S2E). Elevated fat accumulations were also
150 observed in EHD2 del/del muscle sections (Fig. 2L, M, Fig. S2E, F), indicating a general function of EHD2 in
151 lipid metabolism in many cell types. As no significant differences in EHD2 expression levels and lipid
152 accumulation (Fig. 1, S1 and S2) were found in EHD2 del/+ and C57BL6/N male mice, the following animal
153 experiments were carried out with EHD2 del/+ as control group to EHD2 del/del male mice to reduce
154 animal numbers.

155 Based on the increased lipid accumulation in EHD2-lacking adipocyte tissue, we further
156 investigated if adipocyte differentiation is impaired in EHD2 del/del WAT. However, gene expression
157 analysis of adipogenic marker genes like PPRαγ, Retn or Serpina3k displayed no significant change
158 compared to EHD2 del/+ WAT (Fig. S2G). Furthermore, glucose tolerance was tested in EHD2 del/del mice
159 but did not reveal major differences for blood glucose concentrations after glucose injection compared to
160 EHD2 del/+ mice (Fig. S2H).

161

162 **Increased lipid droplet size in adipocytes lacking EHD2**

163 To explore the function of EHD2 at the cellular level, lipid metabolism was investigated in cultured
164 adipocytes. Primary pre-adipocytes were isolated from WAT of EHD2 del/+ and EHD2 del/del mice and
165 differentiated into mature adipocytes. Oil red O staining revealed increased lipid accumulation in
166 adipocytes lacking EHD2 (Fig. 3A, B). BODIPY staining of these cultures was used to measure the LD size.
167 Undifferentiated EHD2 del/+ and del/del pre-adipocytes had similarly sized LDs. In contrast, enlarged LDs

were found in differentiated EHD2 del/del adipocytes, compared to a moderate size increase in EHD2 del/+ cells (Fig. 3C-E). 3D reconstruction of EHD2 del/del differentiated adipocytes revealed that some LDs even exceeded the volume of the nucleus (Fig. 3C).

Next, we aimed to address the possibility that increased lipid uptake is a secondary effect of EHD2 deletion mediated via putative organ cross-talk. We therefore repeated the experiments with cultivated adipocytes derived from EHD2 cKO flox/flox mice, in which EHD2 expression was down-regulated by expression of Cre recombinase via viral transfection (AAV8). Again, EHD2 removal led to increased LD growth (Fig. 3F), indicating a cell-autonomous function of EHD2 in controlling lipid uptake.

LD growth is mainly mediated by extracellular fatty acid uptake and conversion into triglycerides, whereas increased glucose uptake and *de novo* lipogenesis only play a minor role in this process (Wilfling *et al.*, 2013; Rutkowski, Stern and Scherer, 2015). Fatty acids and lipids are present in high concentrations in fetal bovine serum (FBS). Addition of delipidated FBS during adipocyte differentiation resulted in complete loss of LD in both genotypes (Fig. 3G), whereas glucose-depletion led to a general impairment of adipocyte differentiation. However, enlarged LD could still be observed in KO adipocytes under the latter conditions (Fig. 3G). These data led us to speculate that the increased LD size in EHD2 del/del adipocytes may be a consequence of increased fatty acid uptake.

To test this possibility directly, we monitored the uptake of extracellularly added fatty acids into differentiated adipocytes using BODIPY-labelled dodecanoic acid (FA12) paired with FACS analysis. After 5 min, only a minor fraction of EHD2 del/+ adipocytes displayed intense BODIPY staining (R2, for definition see Fig. 3H, J). This R2 population increased to more than 30% after 60 min of FA12 treatment. EHD2 del/del adipocytes displayed increased BODIPY staining at both early (Fig. 3I, K) and late time points (Fig. 3I, L), indicating accelerated lipid uptake. In line with these experiments, light microscopy imaging revealed a more intense BODIPY staining of EHD2 del/del cells compared to EHD2 del/+ adipocytes after 60 min of fatty acid incubation (Fig. 3M). In contrast, EHD2 del/+ and EHD2 del/del adipocytes did not

192 differ with respect to their ability to take up extracellularly added glucose (Fig. S3A-C). Previously, an
193 involvement of EHD2 in the autophagic engulfment of LD (lipophagy) was suggested (Li *et al.*, 2016).
194 However, inducing starvation by incubation of differentiated adipocytes with Hank's balanced salt
195 solution (HBSS) revealed no differences in the release of stored lipids in EHD2 del/+ and EHD2 del/del
196 adipocytes, and both genotypes displayed similar reductions in lipid accumulation (Fig. S3D). These data
197 indicate that loss of EHD2 does not affect the release of fatty acids or lipophagy, but specifically controls
198 LD size by regulating fatty acid uptake.
199
200 **Loss of EHD2 results in detachment of caveolae from the plasma membrane *in vivo***
201 To address if the absence of EHD2 results in altered caveolar morphology, WAT and BAT were
202 analyzed by electron microscopy (EM). Caveolae in EHD2 del/+ BAT were mostly membrane-bound and
203 displayed the characteristic flask-shaped morphology (Fig. 4A, white arrows, ratio detached/membrane
204 bound caveolae = 0.27). Strikingly, an increased number of caveolae were detached from the plasma
205 membrane in BAT isolated from EHD2 del/del mice compared to EHD2 del/+ controls (Fig. 4A, B, black
206 arrows, ratio detached/membrane bound caveolae = 1.75). The total number of caveolae, as well as the
207 caveolar diameter and size, were unchanged in brown adipocytes lacking EHD2. An increased number of
208 detached caveolae were also observed in EHD2 del/del white adipocytes compared to EHD2 del/+ cells
209 from littermate controls (Fig. 4C, D, black and white arrow heads, ratio detached/membrane bound
210 caveolae (del/del) = 1.2 vs. ratio (del/+) = 0.24). In white adipocytes, a reduced total number of caveolae
211 was determined, while both caveolar size and diameter were increased in EHD2 del/del compared to EHD2
212 del/+ animals (Fig. 4D). Cav1 immunogold labeling confirmed that the round vesicles close the plasma
213 membrane, indeed, were detached caveolae (Fig. 4E). 3D visualization of EHD2 del/del brown adipocyte
214 by electron tomography (ET) further demonstrated that the majority of detached caveolae in 2D EM
215 images were not connected to the plasma membrane (Fig. 4F, G, Movie S1) but localized 20-30 nm

underneath (Fig. 4G a, b), although some caveolae close to the plasma membrane showed thin connections (Fig. 4G b, d, white arrow head). Taken together, EM and ET reveal an increased detachment of caveolae from the plasma membrane in EHD2 del/del adipocytes, suggesting a crucial function for EHD2 in the stabilization of caveolae at the plasma membrane.

Increased caveolar mobility in EHD2 knockout cells

To verify the cell-autonomous EHD2-mediated control of LD size and to further dissect the interplay of caveolar mobility and LD growth at the molecular level, we analyzed mouse embryonic fibroblasts (MEFs) derived from EHD +/+ and EHD2 del/del mice. Oil Red O staining showed increased intensity in EHD2 del/del MEFs after adipogenic differentiation compared to EHD2 +/+ MEFs (Fig. S4A), suggesting increased lipid accumulation. BODIPY staining of EHD2 del/del MEFs revealed enlarged LD sizes after differentiation or treatment with oleic acid for 6 h (Fig. S4B, C). Furthermore, both storage and membrane lipids were largely increased in MEFs lacking EHD2 (Fig. S4D). Re-expression of an EGFP-tagged EHD2 version in MEFs lacking EHD2 completely rescued the observed LD phenotype. In fact, overexpression of EHD2 in +/+ and del/del MEFs reduced the size of LDs compared to EGFP expressing cells (Fig. 5A, B). These data indicate a general and cell autonomous role of EHD2 in the control of LD growth and size.

To test if the observed increased LD size in EHD2 del/del MEFs was dependent on caveolae, MEFs lacking EHD2 were treated with Cav1 siRNA to eliminate caveolae. Indeed, LD sizes in EHD2 KO MEFs were significantly decreased after Cav1 knockdown compared to control siRNA treated cells (Fig. 5C, D), pointing to a crucial role of caveolae in EHD2-controlled LD size.

Next, we investigated caveolar mobility and endocytosis of Cholera toxin subunit B (CTxB) in EHD2 +/+ and del/del MEFs. CTxB can be internalized by multiple pathways including caveolar uptake as well as

239 by clathrin-(and caveolin)-independent carriers (CLICs, Parton and Simons et al., 2007). Strikingly, MEFs
240 lacking EHD2 showed increased CTxB uptake compared to EHD2 +/+ MEFs (Fig. 5E, F).

241 To analyze caveolae dynamics directly, we monitored caveolar movement by total internal
242 reflection fluorescence (TIRF) microscopy. EHD2 +/+ and del/del MEFs were transfected with pCav1-EGFP
243 to label single caveolae. As illustrated in Fig. 5G, regions of moderate Cav1 expression were investigated
244 to ensure that distinct Cav1 spots were observed during the analysis. Live TIRF imaging of EHD2 wt MEFs
245 showed a slow or no continuous movement for the majority of investigated caveolae (Movie S2).
246 However, single caveolae moved along the plasma membrane or left the TIRF illumination zone towards
247 the inside of the cell, indicative of their spontaneous detachment, as previously reported (Moren et al.,
248 2012). Strikingly, movement and velocity of caveolae was greatly increased in EHD2 del/del MEFs (Movie
249 S3), not allowing Cav1 single spots to be tracked. Line scan analysis revealed a greatly reduced number of
250 fixed, non-moving Cav1 spots (referred to as lines in Fig. 5G) in EHD2 del/del MEFs compared to wt cells.
251 Moreover, a larger number of highly mobile Cav1 sparks, reflecting fast moving caveolae, was found in
252 EHD2 del/del cells (Fig. 5G, H). Re-expression of EHD2 in EHD2 del/del MEFs reduced the mobility of
253 caveolae, often leading to their immobilization (Fig. S4E). Collectively, these data show that EHD2 crucially
254 regulates cellular lipid uptake and caveolar mobility.

255

256 **The fatty acid translocase CD36 is involved in EHD2-dependent fatty acid uptake**

257 CD36 had previously been implicated in caveolae-dependent fatty acid uptake (Aboulaich *et al.*,
258 2004; Ring *et al.*, 2006; Eyre *et al.*, 2007). We therefore examined whether the increased fatty acid uptake
259 in EHD2 del/del adipocytes and EHD2 del/del MEFs is mediated by CD36. Initially, we analyzed CD36
260 localization in MEFs using immuno-live stainings (Fig. 6A). Strong CD36 signal was detected at the cell
261 membrane, where a minor pool of CD36 co-localized with Cav1. Partial co-localization of CD36 and Cav1
262 was further confirmed by high-resolution z-stack imaging (Fig. 6A). Both EHD2 KO MEFs (Fig. 6A) and

del/del adipocytes (Fig. S4F) showed a slight reduction in CD36 plasma membrane levels compared to EHD2 expressing cells (Fig. 6C, siRNA negative control), possibly reflecting the increased amount of detached caveolae due to EHD2 loss. Removal of caveolae by Cav1-specific siRNAs treatment resulted in significantly decreased CD36 plasma membrane staining in EHD2 +/+ and del/del MEFs (Fig. 6B, C) suggesting a function of caveolae for CD36 membrane localization (Fig. 6D).

To investigate the causal relationship between the increased LD growth in EHD2 KO MEFs and CD36-mediated lipid uptake, CD36 expression was downregulated in MEFs by treatment with either one of three specific CD36 siRNA, followed by oleic acid application and LD staining. CD36 antibody staining confirmed efficient knockdown of CD36 in EHD2 +/+ and del/del MEFs (Fig. 6E). Strikingly, removal of CD36 in EHD2 +/+ and del/del MEFs dramatically decreased the size of LDs compared to a control siRNA treated cells (Fig. 6E, F). We conclude that the observed enlargement of LDs in cells lacking EHD2 depends on CD36.

Decreased EHD2 expression in genetic obesity models or diet induced obesity

To examine the effect of genetic EHD2 deletion during diet-induced obesity, EHD2 del/+ and del/del mice were fed with a high fat diet (60% kcal fat) for 10 days or 4 months, and the body weight was monitored every 5 days.

Within the first 10 days of high fat feeding, a strong rise in body weight was observed for both genotypes, which was slightly faster in EHD2 del/del mice compared to EHD2 del/+ (Fig. 7A, 0.84 vs. 0.73 g/day). However, in the following days, the differences in the overall body weight disappeared (Fig. 7B). As already observed in EHD2 del/del mice on a standard diet, white and brown adipocytes from EHD2 del/del mice revealed enlarged LD sizes compared to EHD2 del/+ after 10 days on the high fat diet (Fig. 7D). Similar effects were obtained in liver sections (Fig. 7D). After 4 months of high fat feeding, enlarged

lipid accumulation was observed in adipocytes and liver in both genotypes (Fig. S5A, B). Fat mass in EHD2 del/+ and EHD2 del/del mice did not differ after short or long-term high fat feeding (Fig. 7C).

The weight adaptation of both genotypes suggested the occurrence of compensatory mechanisms. First, we looked for changes of adiponectin, leptin and insulin blood levels but did not detect any significant difference in mice lacking EHD2 compared to EHD2 del/+ mice after 4 months of high fat feeding or under standard diet (Fig. S6A, B). Free fatty acid concentration in blood plasma was slightly reduced in EHD2 del/del samples after standard diet indicating increased fatty acid uptake (Fig. S6B).

Already under standard diet, we observed a down-regulation of genes involved in *de novo* lipogenesis in EHD2 del/del vs. EHD2 del/+ mice (Fig. 7E). Similar results were obtained for primary adipocyte cell cultures (Fig. S3E). High fat diet led to a drastic reduction of gene expression in *de novo* lipogenesis like SREBP1 and FAS in WAT obtained from EHD2 del/del mice, suggesting that downregulation of lipogenesis is an active mechanism that partially compensates for the enhanced lipid uptake (Fig. 7F). Remarkably, EHD2 expression was essentially absent in WAT obtained from EHD2 del/+ mice following a 4 months high fat diet (Fig. 7G). This may explain the similar phenotypes of EHD2 del/+ and EHD2 del/del mice following a long-term high fat diet (Fig. 7B, Fig. S5).

Based on these observations, EHD2 expression was investigated in two obesity-related mouse models, ob/ob and NZO (Kleinert *et al.*, 2018). Indeed, WAT obtained from ob/ob and NZO mice showed reduced EHD2 expression compared to C57BL6/N mice fed by standard diet (Fig. 7H). When investigating adipocytes from ob/ob mice, a higher proportion of detached caveolae were found in the obesity mouse model (ratio detached/membrane bound caveolae = 1.4 vs. 0.35 in C57BL6/N mice fed with standard diet, Fig. 7I-J). Taken together, these data indicate that EHD2 expression is highly regulated by lipid uptake and load and suggest that EHD2-mediated caveolar dynamics is altered in obesity.

Discussion

Here, we identify EHD2 as a negative regulator of caveolae-dependent lipid uptake. In caveolae containing cells, like adipocytes, muscle cells or fibroblasts, loss of EHD2 resulted in increased lipid accumulation, which was observed in the whole organism as well as in cell culture-based experiments. Loss of EHD2 was associated with the detachment of caveolae from the plasma membrane, higher caveolar mobility and increased uptake of lipids and other caveolar substrates, such as CTxB. We demonstrate that the fatty acid translocase CD36 participates in this EHD2-dependent lipid uptake pathway. Furthermore, obese mouse models and mice exposed to a long-term high fat diet exhibit decreased EHD2 expression in WAT. Thus, our study reveals a cell-autonomous lipid uptake route that involves CD36 and caveolae, is controlled by EHD2 and modified by metabolic conditions.

For some time, caveolae have been implicated in lipid uptake. Thus, mice lacking caveolae showed reduced fat mass and did not develop any form of obesity. In addition, Pohl et al. (2005) observed decreased oleate uptake after expression of a dominant-negative Cav1 mutant. The EHD2 KO mouse model, described here, revealed the opposite phenotype, e.g. a caveolae gain-of-function *in vivo* model. In EHD2 KO mice, caveolae were more often detached from the plasma membrane and showed a higher mobility and faster lipid uptake, resulting in enlarged LDs. Unlike in Cav1 over-expressing mice (Briand *et al.*, 2014), which also show increased fatty acid uptake, the number of caveolae remained unchanged in EHD2 KO mice. This supports a model in which not only caveolae numbers, but also caveolar dynamics play a crucial role in this process (see model in Fig. 7K). Furthermore, such idea is in line with our structural findings that EHD2 can form ring-like oligomers that may stabilize the neck of caveolae (Daumke et al, 2007; Shah et al., 2014; Melo et al., 2017; Hoernke et al., 2017), thereby restricting caveolar mobility (Morén *et al.*, 2012; Stoeber *et al.*, 2012). Based on studies in EHD2 KO NIH 3T3 cell line, Yeow et al. (2017) suggested that EHD1 and/or EHD4 could rescue loss of EHD2 during its role in membrane protection. However, we did not find rescue of caveolae detachment and lipid uptake in EHD2 KO cells by other EHD family members.

We show that CD36 partially co-localizes with caveolae and is involved in EHD2-mediated lipid uptake. Previous Cav1 KO studies already showed mis-localization of CD36 and impaired fatty acid uptake in MEFs lacking caveolae (Ring *et al.*, 2006). CD36 belongs to a superfamily of integral membrane protein, the CD36 scavenger receptors, which also include the lysosomal integral membrane protein II (LIMP 2). The structure of the latter revealed a large hydrophobic tunnel in the conserved globular domain which was suggested to deliver lipids in the outer membrane (Hsieh *et al.*, 2016). The specific lipid environment of caveolae, including a high proportion of cholesterol, may support CD36-mediated lipid uptake in caveolae. Our data support the idea that caveolae shuttling between the plasma membrane and intracellular compartments is involved in lipid uptake (as illustrated in Fig. 7K). Conventional caveolae internalization follows the endosomal pathway from early to late endosomes and finally to lysosomes (Pelkmans *et al.*, 2004; Hayer *et al.*, 2010). However, initial cellular fatty acid accumulation within LDs can be much faster (minutes) (Kuerschner, Moessinger and Thiele, 2008) compared to the caveolar turnover in lysosomes (one hour), suggesting an involvement of alternative pathways. Notably, LDs form at the membrane of the endoplasmic reticulum (ER) (Pol, Gross and Parton, 2014; Wilfling *et al.*, 2014; Barneda and Christian, 2017), and it was proposed before that caveolae could translocate to the ER and form contact sites (Le *et al.*, 2002; Le, 2003). Furthermore, a role of Cav1 in LD formation has been suggested (Ostermeyer *et al.*, 2001; Schlegel, Arvan and Lisanti, 2001; Robenek *et al.*, 2004). With the EHD2 KO mice, we have developed a suitable model to explore the molecular components of the caveolae-dependent lipid uptake pathway.

The loss of EHD2 on the cellular level led to increased fat deposits on the organismic level, which was particularly evident in older animals. The observed phenotype based on the global loss of EHD2 could be influenced by organ-organ interactions (Stern, Rutkowski and Scherer, 2016). However, we did not find any evidence for differences in adipocyte derived secretory factors, such as adiponectin (Fig. S6). Furthermore, increased lipid uptake was dependent on caveolae, as shown by Cav1 knockdown

358 experiments, and lipid droplet growth could specifically be induced by viral transfection of Cre
359 recombinase in EHD2 cKO flox/flox, but not in flox/wt adipocytes. Thus, increased lipid uptake is caused
360 by a cell-autonomous, caveolae-dependent mechanism. As the WAT distribution and lipid accumulation
361 is known to differ in male and female mice, further studies are required to analyze potential sex-specific
362 differences in EHD2-dependent lipid uptake.

363 Despite the observed LD accumulation in mice lacking EHD2 (under standard and high fat diet),
364 the body weight and overall fat mass of EHD2 del/del and EHD2 del/+ mice were not altered, suggesting
365 metabolic compensation. In line with this idea, EHD2 del/del WAT and cultivated EHD2 del/del adipocytes
366 showed a significant reduction in expression levels of genes involved in *de novo* lipogenesis like SREBP1
367 or FAS indicating a strong downregulation of glucose-dependent fatty acid production in fat cells. Similar
368 compensatory mechanisms were noted in patients suffering from obesity (Eissing *et al.*, 2013; Guiu-Jurado
369 *et al.*, 2015; Solinas, Borén and Dulloo, 2015). Even with elevated fat content in the adipose tissues, liver
370 and skeletal muscle EHD2 del/del mice did not develop an insulin resistance as indicated by the normal
371 glucose tolerance.

372 Remarkably, the expression levels of EHD2 in WAT of two obese mouse models (ob/ob and NZO
373 mice) and of EHD2 del/+ mice treated with a long-term high fat diet were significantly lower than in
374 C57BL6/N or EHD2 del/+ mice under standard diet, resulting in detachment of caveolae. Thus, expression
375 of EHD2 appears to negatively correlate with adipocyte size, therefore reflecting the situation in the EHD2
376 KO mouse (see also (Sonne *et al.*, 2017)). Consistent with this observation, it was previously reported that
377 increased Cav1 expression and caveolae number were detected in patients suffering from obesity or T2D,
378 and also in obesity rat models (Catalán *et al.*, 2008; Grayson *et al.*, 2013). We speculate that an imbalance
379 in number, life-time and mobility of caveolae appears to accompany and maybe actively contribute to the
380 development and progression of obesity. Accordingly, pharmacological approaches to enhance EHD2

expression or its stabilization at the plasma membrane could reduce lipid uptake and consequently help to treat obesity in patients.

In conclusion, our study reveals a conserved cellular lipid uptake pathway that involves caveolae and CD36 and is controlled by EHD2.

Acknowledgments

We thank Petra Stallerow for taking care of the EHD2 delta E3 mouse strain, Karin Jacobi for advice with the animal application, Arnd Heuser and the pathophysiology facility for measuring the body composition, Vivian Schulz for helping with the genotyping of the mice, Claudio Shah for purifying the EHD2 antiserum, and the advanced light imaging facility at MDC for technical support. The authors acknowledge financial support from the Deutsche Forschungsgemeinschaft (DFG; SFB 958/A7 to V.H., A12 to O.D., A13 to A.S.) and support by The Initiative and Networking Fund of the Helmholtz Association.

Author Contributions

C.M. planned, performed and analyzed all experiments if not otherwise indicated. C.M. and O.D. wrote the manuscript, with input from all authors. S.K. performed and analyzed all EM imaging, C.M. analyzed EM images, S.K. and C.M. performed and analyzed ET. I.L. generated the EHD2 KO mouse model and performed in situ hybridization. W.J. analyzed blood plasma markers and EHD2 expression in obesity mouse models. M.L. helped during TIRF imaging and discussed experiments, A.M. isolated primary MEF and performed the EHD2 Western Blot. E.L. performed lipid droplet staining experiments after Cav1 knockdown. A.S., V.H., R.L., C.B. and D.N.M. discussed potential experiments and the manuscript. O.D. wrote the mouse animal application with help of D.N.M. and C.M.

Declaration of Interests

405 The authors declare no competing interests.

406

407 **References**

408 Aboulaich, N., Vainonen, J. P., Stralfors, P. and Vener, A. V (2004) 'Vectorial proteomics reveal targeting,
409 phosphorylation and specific fragmentation of polymerase I and transcript release factor (PTRF) at the
410 surface of caveolae in human adipocytes.', *The Biochemical journal*, 383(Pt 2), pp. 237–48. doi:
411 10.1042/BJ20040647.

412 Barneda, D. and Christian, M. (2017) 'Lipid droplet growth: regulation of a dynamic organelle', *Current*
413 *Opinion in Cell Biology*. Elsevier Ltd, 47, pp. 9–15. doi: 10.1016/j.ceb.2017.02.002.

414 Briand, N., Prado, C., Mabilleau, G., Lasnier, F., Le Liepvre, X., Covington, J. D., Ravussin, E., Le Lay, S. and
415 Dugail, I. (2014) 'Caveolin-1 expression and cavin stability regulate caveolae dynamics in adipocyte lipid
416 store fluctuation', *Diabetes*, 63(12), pp. 4032–4044. doi: 10.2337/db13-1961.

417 Catalán, V., Gómez-Ambrosi, J., Rodríguez, A., Silva, C., Rotellar, F., Gil, M. J., Cienfuegos, J. A., Salvador,
418 J. and Frühbeck, G. (2008) 'Expression of caveolin-1 in human adipose tissue is upregulated in obesity
419 and obesity-associated type 2 diabetes mellitus and related to inflammation', *Clinical Endocrinology*,
420 68(2), pp. 213–219. doi: 10.1111/j.1365-2265.2007.03021.x.

421 Cham, B. E. and Knowles, B. R. (1976) 'A solvent system for delipidation of plasma or serum without
422 protein precipitation.', *Journal of lipid research*, 17, pp. 176–181.

423 Cheng, J. P. X. and Nichols, B. J. (2016) 'Caveolae : One Function or Many ?', *Trends in cell biology*.
424 Elsevier Ltd, 26(3), pp. 177–189.

425 Daumke, O., Lundmark, R., Vallis, Y., Martens, S., Butler, P. J. G. and McMahon, H. T. (2007)
426 'Architectural and mechanistic insights into an EHD ATPase involved in membrane remodelling.', *Nature*,
427 449(7164), pp. 923–7. doi: 10.1038/nature06173.

428 Ding, S. Y., Lee, M. J., Summer, R., Liu, L., Fried, S. K. and Pilch, P. F. (2014) 'Pleiotropic effects of cavin-1
429 deficiency on lipid metabolism', *Journal of Biological Chemistry*, 289(12), pp. 8473–8483. doi:
430 10.1074/jbc.M113.546242.

431 Drab, M., Verkade, P., Elger, M., Kasper, M., Lohn, M., Lauterbach, B., Menne, J., Lindschau, C., Mende,
432 F., Luft, F. C., Schedl, A., Haller, H. and Kurzchalia, T. V (2001) 'Loss of caveolae, vascular dysfunction, and
433 pulmonary defects in caveolin-1 gene-disrupted mice', *Science*, 293(5539), pp. 2449–2452. doi:
434 10.1126/science.1062688.

435 Dubikovskaya, E., Chudnovskiy, R., Karateev, G., Park, H. M. and Stahl, A. (2014) 'Measurement of long-
436 chain fatty acid uptake into adipocytes', *Methods Enzymol*, 538(1), pp. 107–134. doi:
437 10.3816/CLM.2009.n.003.Novel.

438 Eissing, L., Scherer, T., Tödter, K., Knippschild, U., Greve, J. W., Buurman, W. a, Pinnschmidt, H. O.,
439 Rensen, S. S. and Wolf, A. M. (2013) 'De novo lipogenesis in human fat and liver is linked to ChREBP- β
440 and metabolic health', *Nature Communications*, 4, pp. 1528–1539. doi: 10.1038/ncomms2537.De.

441 Eyre, N. S., Cleland, L. G., Tandon, N. N. and Mayrhofer, G. (2007) 'Importance of the carboxyl terminus
442 of FAT/CD36 for plasma membrane localization and function in long-chain fatty acid uptake', *Journal of*
443 *Lipid Research*, 48(3), pp. 528–542. doi: 10.1194/jlr.M600255-JLR200.

444 Grayson, T. H., Chadha, P. S., Bertrand, P. P., Chen, H., Morris, M. J., Senadheera, S., Murphy, T. V. and
445 Sandow, S. L. (2013) 'Increased caveolae density and caveolin-1 expression accompany impaired NO-
446 mediated vasorelaxation in diet-induced obesity', *Histochemistry and Cell Biology*, 139(2), pp. 309–321.
447 doi: 10.1007/s00418-012-1032-2.

448 Guiu-Jurado, E., Auguet, T., Berlanga, A., Aragonès, G., Aguilar, C., Sabench, F., Armengol, S., Porras, J.
449 A., Martí, A., Jorba, R., Hernández, M., del Castillo, D. and Richart, C. (2015) 'Downregulation of de novo
450 fatty acid synthesis in subcutaneous adipose tissue of moderately obesewomen', *International Journal*
451 *of Molecular Sciences*, 16(12), pp. 29911–29922. doi: 10.3390/ijms161226206.

452 Hansen, C. G., Howard, G. and Nichols, B. J. (2011) 'Pacsin 2 is recruited to caveolae and functions in
453 caveolar biogenesis.', *Journal of cell science*, 124(Pt 16), pp. 2777–2785. doi: 10.1242/jcs.084319.

454 Hansen, C. G., Shvets, E., Howard, G., Riento, K. and Nichols, B. J. (2013) 'Deletion of cavin genes reveals
455 tissue-specific mechanisms for morphogenesis of endothelial caveolae', *Nature Communications*. Nature
456 Publishing Group, 4(May), pp. 1813–1831. doi: 10.1038/ncomms2808.

457 Hayer, A., Stoeber, M., Ritz, D., Engel, S., Meyer, H. H. and Helenius, A. (2010) 'Caveolin-1 is
458 ubiquitinated and targeted to intralumenal vesicles in endolysosomes for degradation', *Journal of Cell*
459 *Biology*, 191(3), pp. 615–629. doi: 10.1083/jcb.201003086.

460 Hill, M. M., Bastiani, M., Luetterforst, R., Kirkham, M., Kirkham, A., Nixon, S. J., Walser, P., Abankwa, D.,
461 Oorschot, V. M. J., Martin, S., Hancock, J. F. and Parton, R. G. (2008) 'PTRF-Cavin, a Conserved
462 Cytoplasmic Protein Required for Caveola Formation and Function', *Cell*, 132(1), pp. 113–124. doi:
463 10.1016/j.cell.2007.11.042.

464 Hoernke, M., Mohan, J., Larsson, E., Blomberg, J., Kahra, D., Westenhoff, S., Schwieger, C. and
465 Lundmark, R. (2017) 'EHD2 restrains dynamics of caveolae by an ATP-dependent, membrane-bound,
466 open conformation.', *Proceedings of the National Academy of Sciences of the United States of America*,
467 114(22), pp. E4360–E4369. doi: 10.1073/pnas.1614066114.

468 Hsieh, F. L., Turner, L., Bolla, J. R., Robinson, C. V., Lavstsen, T. and Higgins, M. K. (2016) 'The structural
469 basis for CD36 binding by the malaria parasite', *Nature Communications*. Nature Publishing Group,
470 7(May), pp. 1–11. doi: 10.1038/ncomms12837.

471 Ju, H., Zou, R., Venema, V. J. and Venema, R. C. (1997) 'Direct Interaction of Endothelial Nitric-oxide
472 Synthase and Caveolin-1 Inhibits Synthase Activity', *The Journal of biological chemistry*, 272(30), pp.
473 18522–18525.

474 Kärgel, E., Menzel, R., Honeck, H., Vogel, F., Böhmer, a and Schunck, W. H. (1996) 'Candida maltosa
475 NADPH-cytochrome P450 reductase: cloning of a full-length cDNA, heterologous expression in
476 Saccharomyces cerevisiae and function of the N-terminal region for membrane anchoring and
477 proliferation of the endoplasmic reticulum.', *Yeast (Chichester, England)*, 12(4), pp. 333–348. doi:
478 10.1002/(SICI)1097-0061(19960330)12:4<333::AID-YEA915>3.0.CO;2-C.

479 Kleinert, M., Clemmensen, C., Hofmann, S. M., Moore, M. C., Renner, S., Woods, S. C., Huypens, P.,
480 Beckers, J., De Angelis, M. H., Schürmann, A., Bakhti, M., Klingenspor, M., Heiman, M., Cherrington, A.
481 D., Ristow, M., Lickert, H., Wolf, E., Havel, P. J., Müller, T. D. and Tschöp, M. H. (2018) 'Animal models of
482 obesity and diabetes mellitus', *Nature Reviews Endocrinology*. Nature Publishing Group, 14(3), pp. 140–
483 162. doi: 10.1038/nrendo.2017.161.

484 Kluth, O., Matzke, D., Kamitz, A., Jähnert, M., Vogel, H., Scherneck, S., Schulze, M., Staiger, H., Machicao,
485 F., Häring, H.-U., Joost, H.-G. and Schürmann, A. (2015) 'Identification of Four Mouse Diabetes Candidate
486 Genes Altering β-Cell Proliferation', *PLOS Genetics*. Edited by G. S. Barsh, 11(9), p. e1005506. doi:

10.1371/journal.pgen.1005506.

Kovtun, O., Tillu, V. A., Ariotti, N., Parton, R. G. and Collins, B. M. (2015) 'Cavin family proteins and the assembly of caveolae', *Journal of cell science*, 128(7), pp. 1269–1278. doi: 10.1242/jcs.167866.

Kuerschner, L., Moessinger, C. and Thiele, C. (2008) 'Imaging of lipid biosynthesis: How a neutral lipid enters lipid droplets', *Traffic*, 9(3), pp. 338–352. doi: 10.1111/j.1600-0854.2007.00689.x.

Le, P. U. (2003) 'Distinct caveolae-mediated endocytic pathways target the Golgi apparatus and the endoplasmic reticulum', *Journal of Cell Science*, 116(6), pp. 1059–1071. doi: 10.1242/jcs.00327.

Le, P. U., Guay, G., Altschuler, Y. and Nabi, I. R. (2002) 'Caveolin-1 is a negative regulator of caveolae-mediated endocytosis to the endoplasmic reticulum', *Journal of Biological Chemistry*, 277(5), pp. 3371–3379. doi: 10.1074/jbc.M111240200.

Li, Z., Schulze, R. J., Weller, S. G., Krueger, E. W., Schott, M. B., Zhang, X., Casey, C. A., Liu, J., Stöckli, J., James, D. E. and McNiven, M. A. (2016) 'A novel Rab10-EHBP1-EHD2 complex essential for the autophagic engulfment of lipid droplets', *Science Advances*, 2(12), pp. 1–16.

Liu, L., Brown, D., McKee, M., LeBrasseur, N. K., Yang, D., Albrecht, K. H., Ravid, K. and Pilch, P. F. (2008) 'Deletion of Cavin/PTRF Causes Global Loss of Caveolae, Dyslipidemia, and Glucose Intolerance', *Cell Metabolism*, 8(4), pp. 310–317. doi: 10.1016/j.cmet.2008.07.008.

Liu, L., Hansen, C. G., Honeyman, B. J., Nichols, B. J. and Pilch, P. F. (2014) 'Cavin-3 knockout mice show that cavin-3 is not essential for caveolae formation, for maintenance of body composition, or for glucose tolerance', *PLoS ONE*, 9(7), pp. 1–8. doi: 10.1371/journal.pone.0102935.

Liu, P., Jenkins, N. A., Copeland, N. G., Liu, P., Jenkins, N. A. and Copeland, N. G. (2003) 'A Highly Efficient Recombineering-Based Method for Generating Conditional Knockout Mutations', *Genome Research*, 13, pp. 476–484. doi: 10.1101/gr.749203.

Ludwig, A., Howard, G., Mendoza-Topaz, C., Deerinck, T., Mackey, M., Sandin, S., Ellisman, M. H. and Nichols, B. J. (2013) 'Molecular Composition and Ultrastructure of the Caveolar Coat Complex', *PLoS Biology*, 11(8). doi: 10.1371/journal.pbio.1001640.

Ludwig, A., Nichols, B. J. and Sandin, S. (2016) 'Architecture of the caveolar coat complex.', *Journal of cell science*, pp. 3077–3083. doi: 10.1242/jcs.191262.

Martin, S., Fernandez-Rojo, M. A., Stanley, A. C., Bastiani, M., Okano, S., Nixon, S. J., Thomas, G., Stow, J. L. and Parton, R. G. (2012) 'Caveolin-1 Deficiency Leads to Increased Susceptibility to Cell Death and Fibrosis in White Adipose Tissue: Characterization of a Lipodystrophic Model', *PLoS ONE*, 7(9), pp. 1–9. doi: 10.1371/journal.pone.0046242.

Mehlem, A., Hagberg, C. E., Muhl, L., Eriksson, U. and Falkevall, A. (2013) 'Imaging of neutral lipids by oil red O for analyzing the metabolic status in health and disease', *Nature Protocols*, 8(6), pp. 1149–1154. doi: 10.1038/nprot.2013.055.

Melo, A. A., Hegde, B. G., Shah, C., Larsson, E., Isas, J. M., Kunz, S., Lundmark, R., Langen, R. and Daumke, O. (2017) 'Structural insights into the activation mechanism of dynamin-like EHD ATPases', *Proceedings of the National Academy of Sciences*, 114(22), pp. 5629–5634. doi: 10.1073/pnas.1614075114.

Mohan, J., Moren, B., Larsson, E., Holst, M. R. and Lundmark, R. (2015) 'Cavin3 interacts with cavin1 and caveolin1 to increase surface dynamics of caveolae', *Journal of Cell Science*, 128(5), pp. 979–991. doi: 10.1242/jcs.161463.

Morén, B., Shah, C., Howes, M. T., Schieber, N. L., McMahon, H. T., Parton, R. G., Daumke, O. and

528 Lundmark, R. (2012) 'EHD2 regulates caveolar dynamics via ATP-driven targeting and oligomerization.',
529 *Molecular biology of the cell*, 23(7), pp. 1316–29. doi: 10.1091/mbc.E11-09-0787.

530 NIH Accelerating Medicines Partnership (2014) *Type 2 Diabetes Knowledge Portal*,
531 *http://www.type2diabetesgenetics.org*.

532 Ostermeyer, A. G., Paci, J. M., Zeng, Y., Lublin, D. M., Munro, S. and Brown, D. A. (2001) 'Accumulation of
533 caveolin in the endoplasmic reticulum redirects the protein to lipid storage droplets', *Journal of Cell*
534 *Biology*, 152(5), pp. 1071–1078. doi: 10.1083/jcb.152.5.1071.

535 Pelkmans, L., Bürli, T., Zerial, M. and Helenius, A. (2004) 'Caveolin-stabilized membrane domains as
536 multifunctional transport and sorting devices in endocytic membrane traffic', *Cell*, 118(6), pp. 767–780.
537 doi: 10.1016/j.cell.2004.09.003.

538 Pohl, J., Ring, A., Ehehalt, R., Schulze-Bergkamen, H., Schad, A., Verkade, P. and Stremmel, W. (2004)
539 'Long-Chain Fatty Acid Uptake into Adipocytes Depends on Lipid Raft Function', *Biochemistry*, 43(14), pp.
540 4179–4187. doi: 10.1021/bi035743m.

541 Pol, A., Gross, S. P. and Parton, R. G. (2014) 'Biogenesis of the multifunctional lipid droplet: Lipids,
542 proteins, and sites', *Journal of Cell Biology*, 204(5), pp. 635–646. doi: 10.1083/jcb.201311051.

543 Razani, B., Combs, T. P., Wang, X. B., Frank, P. G., Park, D. S., Russell, R. G., Li, M., Tang, B., Jelicks, L. A.,
544 Scherer, P. E. and Lisanti, M. P. (2002) 'Caveolin-1-deficient mice are lean, resistant to diet-induced
545 obesity, and show hypertriglyceridemia with adipocyte abnormalities', *Journal of Biological Chemistry*,
546 277(10), pp. 8635–8647. doi: 10.1074/jbc.M110970200.

547 Ring, A., Le Lay, S., Pohl, J., Verkade, P. and Stremmel, W. (2006) 'Caveolin-1 is required for fatty acid
548 translocase (FAT/CD36) localization and function at the plasma membrane of mouse embryonic
549 fibroblasts', *Biochimica et Biophysica Acta - Molecular and Cell Biology of Lipids*. Elsevier B.V., 1761(4),
550 pp. 416–423. doi: 10.1016/j.bbalip.2006.03.016.

551 Robenek, M. J., Severs, N. J., Schlattmann, K., Plenz, G., Zimmer, K. P., Troyer, D. and Robenek, H. (2004)
552 'Lipids partition caveolin-1 from ER membranes into lipid droplets: updating the model of lipid droplet
553 biogenesis.', *The FASEB journal : official publication of the Federation of American Societies for*
554 *Experimental Biology*, 18(7), pp. 866–868. doi: 10.1096/fj.03-0782fje.

555 Rutkowski, J. M., Stern, J. H. and Scherer, P. E. (2015) 'The cell biology of fat expansion', *Journal of Cell*
556 *Biology*, 208(5), pp. 501–512. doi: 10.1083/jcb.201409063.

557 Schlegel, A., Arvan, P. and Lisanti, M. P. (2001) 'Caveolin-1 binding to endoplasmic reticulum membranes
558 and entry into the regulated secretory pathway are regulated by serine phosphorylation. Protein sorting
559 at the level of the endoplasmic reticulum', *Journal of Biological Chemistry*, 276(6), pp. 4398–4408. doi:
560 10.1074/jbc.M005448200.

561 Seemann, E., Sun, M., Krueger, S., Tröger, J., Hou, W., Haag, N., Schüler, S., Westermann, M., Huebner,
562 C. A., Romeike, B., Kessels, M. M. and Qualmann, B. (2017) 'Deciphering caveolar functions by syndapin
563 III KO-mediated impairment of caveolar invagination', *eLife*, 6, pp. 1–37. doi: 10.7554/eLife.29854.

564 Senju, Y., Itoh, Y., Takano, K., Hamada, S. and Suetsugu, S. (2011) 'Essential role of PACSIN2/syndapin-II
565 in caveolae membrane sculpting', *Journal of Cell Science*, 124(12), pp. 2032–2040. doi:
566 10.1242/jcs.086264.

567 Shah, C., Hegde, B. G., Morén, B., Behrmann, E., Mielke, T., Moenke, G., Spahn, C. M. T., Lundmark, R.,
568 Daumke, O. and Langen, R. (2014) 'Structural insights into membrane interaction and caveolar targeting
569 of dynamin-like EHD2', *Structure*, 22(3), pp. 409–420. doi: 10.1016/j.str.2013.12.015.

570 Shvets, E., Bitsikas, V., Howard, G., Hansen, C. G. and Nichols, B. J. (2015) 'Dynamic caveolae exclude
571 bulk membrane proteins and are required for sorting of excess glycosphingolipids.', *Nature*
572 *communications*. Nature Publishing Group, 6, pp. 6867–6883. doi: 10.1038/ncomms7867.

573 Sinha, B., Köster, D., Ruez, R., Gonnord, P., Bastiani, M., Abankwa, D., Stan, R. V., Butler-Browne, G.,
574 Vedie, B., Johannes, L., Morone, N., Parton, R. G., Raposo, G., Sens, P., Lamaze, C. and Nassoy, P. (2011)
575 'Cells respond to mechanical stress by rapid disassembly of caveolae', *Cell*, 144(3), pp. 402–413. doi:
576 10.1016/j.cell.2010.12.031.

577 Solinas, G., Borén, J. and Dulloo, A. G. (2015) 'De novo lipogenesis in metabolic homeostasis: More
578 friend than foe?', *Molecular Metabolism*. Elsevier GmbH, 4(5), pp. 367–377. doi:
579 10.1016/j.molmet.2015.03.004.

580 Sonne, S. B., Yadav, R., Yin, G., Dalgaard, M. D., Myrmel, L. S., Gupta, R., Wang, J., Madsen, L., Kajimura,
581 S. and Kristiansen, K. (2017) 'Obesity is associated with depot-specific alterations in adipocyte DNA
582 methylation and gene expression', *Adipocyte*. Taylor & Francis, (May), pp. 1–10. doi:
583 10.1080/21623945.2017.1320002.

584 Sotgia, F., Razani, B., Bonuccelli, G., Schubert, W., Battista, M., Lee, H., Capozza, F., Schubert, A. L.,
585 Minetti, C., Buckley, J. T. and Lisanti, M. P. (2002) 'Intracellular retention of glycosylphosphatidyl
586 inositol-linked proteins in caveolin-deficient cells.', *Molecular and cellular biology*, 22(11), pp. 3905–
587 3926. doi: 10.1128/MCB.22.11.3905-3926.2002.

588 Stern, J. H., Rutkowski, J. M. and Scherer, P. E. (2016) 'Review Adiponectin , Leptin , and Fatty Acids in
589 the Maintenance of Metabolic Homeostasis through Adipose Tissue Crosstalk', *Cell Metabolism*. Elsevier
590 Inc., 23(5), pp. 770–784. doi: 10.1016/j.cmet.2016.04.011.

591 Stoeber, M., Schellenberger, P., Siebert, C. A., Leyrat, C., Helenius, A. and Grünewald, K. (2016) 'Model
592 for the architecture of caveolae based on a flexible, net-like assembly of Cavin1 and Caveolin discs.',
593 *Proceedings of the National Academy of Sciences of the United States of America*, p. 201616838. doi:
594 10.1073/pnas.1616838113.

595 Stoeber, M., Stoeck, I. K., Hänni, C., Bleck, C. K. E., Balistreri, G. and Helenius, A. (2012) 'Oligomers of the
596 ATPase EHD2 confine caveolae to the plasma membrane through association with actin', *The EMBO*
597 *Journal*, 31(10), pp. 2350–2364. doi: 10.1038/emboj.2012.98.

598 Torrino, S., Shen, W. W., Blouin, C. M., Mani, S. K., Lesegno, C. V. De and Bost, P. (2018) 'EHD2 is a
599 mechanotransducer connecting caveolae dynamics with gene transcription', pp. 1–14.

600 Uhlén, M., Fagerberg, L., Hallström, B. M., Lindskog, C., Oksvold, P., Mardinoglu, A., Sivertsson, Å.,
601 Kampf, C., Sjöstedt, E., Asplund, A., Olsson, I., Edlund, K., Lundberg, E., Navani, S., Szigyarto, C. A.,
602 Odeberg, J., Djureinovic, D., Takanen, J. O., Hober, S., Alm, T., Edqvist, P., Berling, H., Tegel, H., Mulder,
603 J., Rockberg, J., Nilsson, P., Schwenk, J. M., Hamsten, M., Feilitzen, K. Von, Forsberg, M., Persson, L.,
604 Johansson, F., Zwahlen, M., Heijne, G. Von, Nielsen, J. and Pontén, F. (2015) 'Tissue-based map of the
605 human proteome', 347(6220). doi: 10.1126/science.1260419.

606 Wilfling, F., Haas, J. T., Walther, T. C. and Jr, R. V. F. (2014) 'Lipid droplet biogenesis', *Current Opinion in*
607 *Cell Biology*. Elsevier Ltd, 29(1), pp. 39–45. doi: 10.1016/j.ceb.2014.03.008.

608 Wilfling, F., Wang, H., Haas, J. T., Krahmer, N., Gould, T. J., Uchida, A., Cheng, J. X., Graham, M.,
609 Christiano, R., Fröhlich, F., Liu, X., Buhman, K. K., Coleman, R. A., Bewersdorf, J., Farese, R. V. and
610 Walther, T. C. (2013) 'Triacylglycerol synthesis enzymes mediate lipid droplet growth by relocalizing
611 from the ER to lipid droplets', *Developmental Cell*, 24(4), pp. 384–399. doi:
612 10.1016/j.devcel.2013.01.013.

613 Wilkinson, D. D. (1993) 'In situ Hybridization. A Practical Approach.', *Genetical Research*. Cambridge
614 University Press, 61(03), p. 234. doi: 10.1017/S0016672300031402.

615

616

Figures

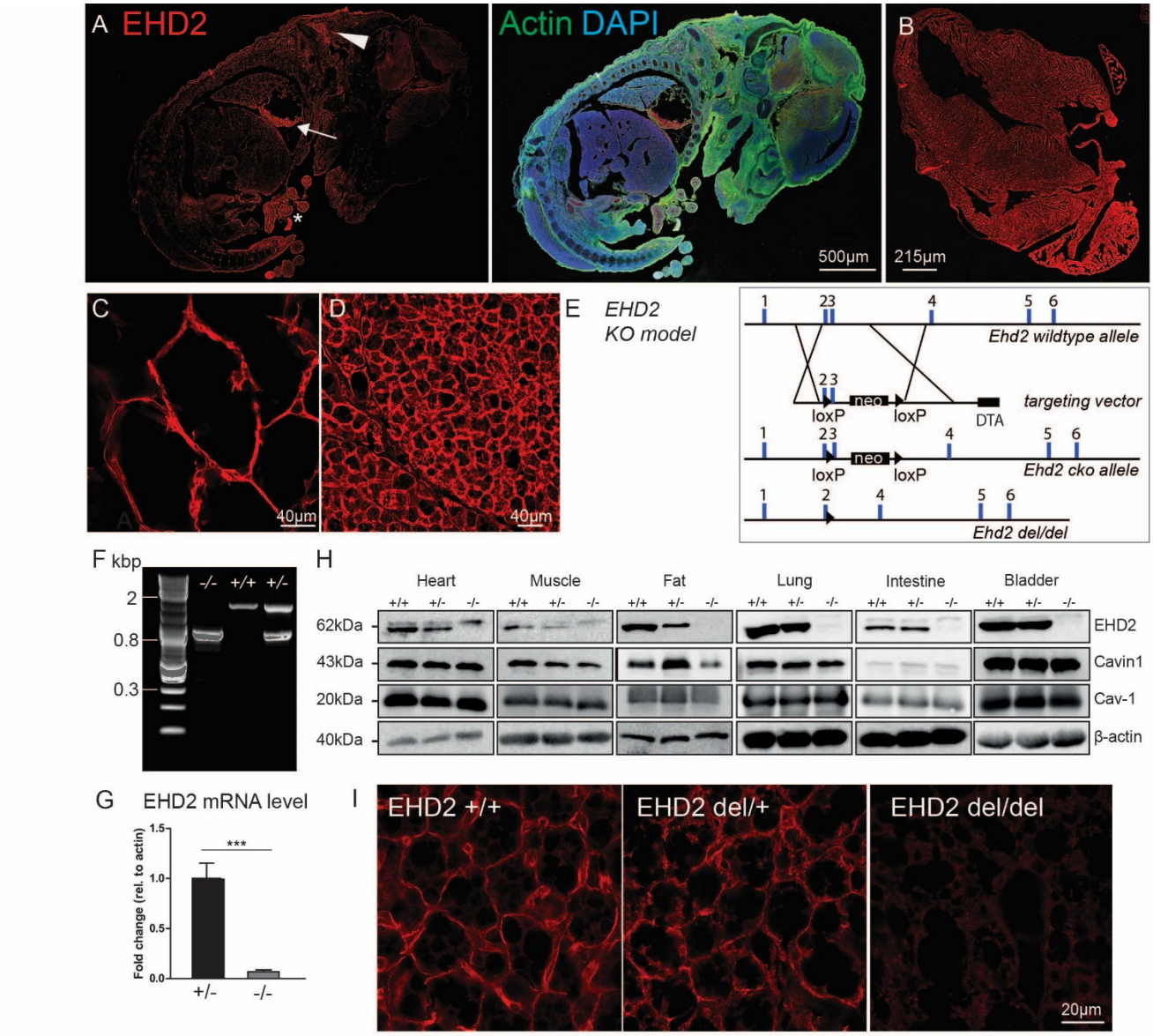

Fig.1 EHD2 is strongly expressed in caveolae containing tissue

A Cryostat section of a C57BL6/N E15 mouse embryo stained against EHD2 (red), actin (green) and the nucleus (Blue, DAPI). White arrowhead indicates BAT, arrow indicates heart, star illustrates umbilical cord. **B-D** Cryostat sections obtained from adult C57BL6/N heart (E), white (F) and brown (G) adipose tissue were stained against EHD2 with an EHD2-specific antibody.

E Generation of the EHD2 KO mouse model. A targeting vector containing a pGK-Neomycin (neo) cassette and loxP sites flanking exon 3 was placed in the EHD2 wt allele. EHD2 del/del mice were obtained by breeding with Cre-deleter mouse strain (DTA - diphtheria toxin A).

F Genotyping of EHD2 delta E3 offspring (wildtype – band size 1,700 bp; EHD2 KO – band size 830 bp).

G EHD2 mRNA level in EHD2 del/+ and EHD2 del/del mice (mRNA from BAT, n = 5, bar column bar graph represents mean + SE, Mann Withney U test, *** $P < 0.0001$).

H Western Blot analysis of different tissues in EHD2+/+, +/- and -/- mice against EHD2, Cav1 and Cavin1.

I EHD2 immuno-staining in BAT cryostat sections from EHD2 +/+, del/+ and del/del mice, see also Fig. S1.

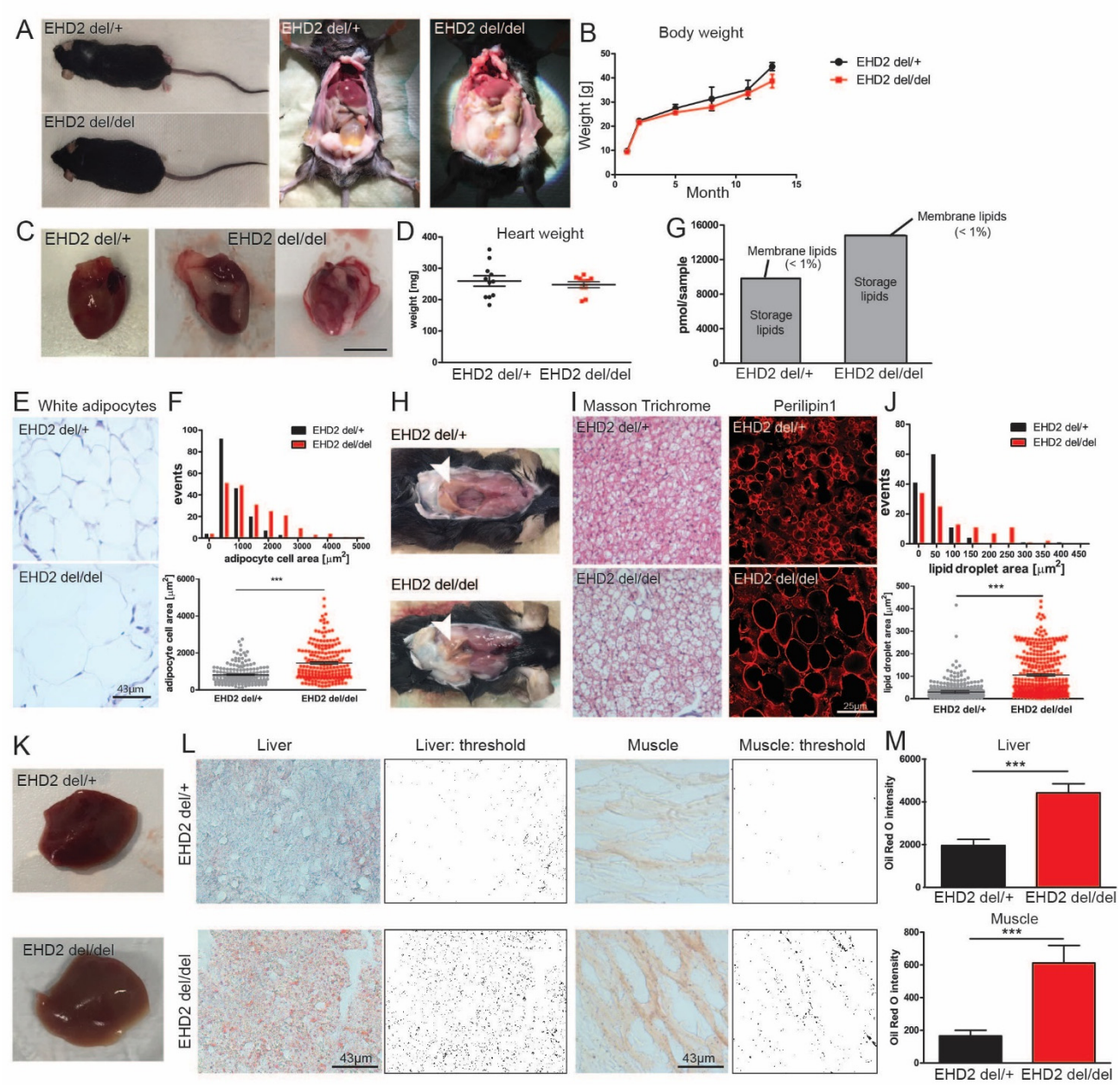

Fig. 2: Increased fat accumulation in EHD2 del/del mice

A-B EHD2 del/+ and EHD2 del/del mice during preparation (A). The body weight was monitored over 12 months (B, n = 7, line graph represents mean +/- SE).

C-D Illustration of EHD2 del/+ and del/del hearts (C, scale bar 1 cm) and its weight (D, n = 10).

E-F Masson Trichrome staining of WAT paraffin sections of EHD2 del/+ and EHD2 del/del. Detailed analysis of the adipocytes cell size (F, n(del/+) = 172/3, n(del/del) = 199/3).

G Lipid composition analysis of 15 µg WAT obtained from EHD2 del/+ or EHD2 del/del mice.

H EHD2 del/del mice showed decreased BAT in the neck region. Instead, WAT was integrated into the BAT depots.

I-J Masson Trichrome staining of EHD2 del/del BAT paraffin sections and BAT cryostat sections stained against the LD coat protein Perilipin1. LD size was measured in BAT cryostat sections (J, n(del/+) = 118/3, n(del/del) = 104/3).

645 **K-M** Representative image of liver obtained from EHD2 del/+ or del/del mice (K). Oil Red O staining of liver
646 and muscle tissue (L, M, n(liver) = 30/3, n(muscle) = 26/3).
647 Box plots indicate each replicate with mean +/- SE, column bar graphs show mean + SE, normal distributed
648 groups were analyzed by t-test, not normally distributed values with Mann Withney U test, * $P<0.05$, ***
649 $P<0.0001$. For comparison to C57BL6/N, see also Fig. S2.

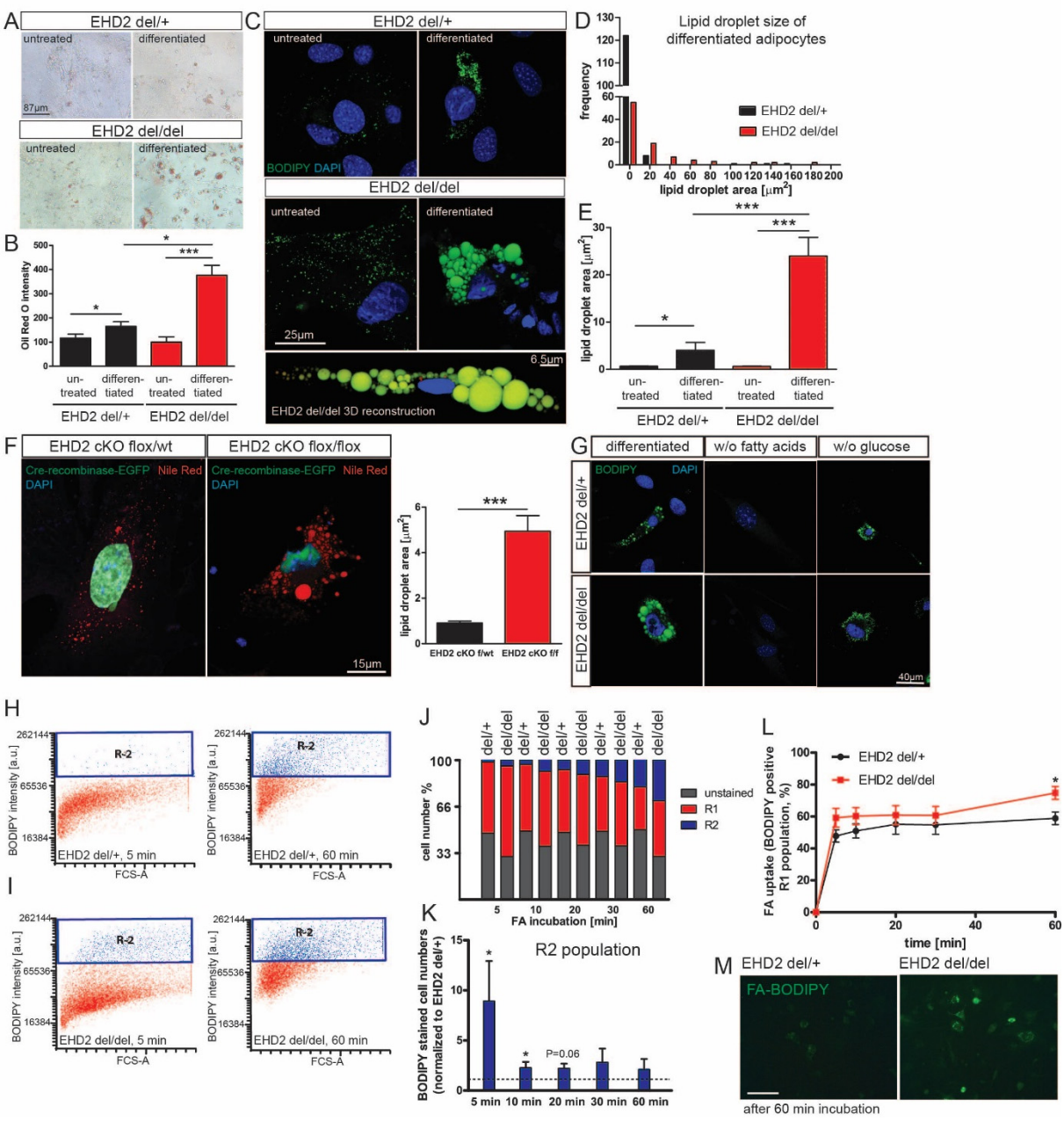

Fig. 3: EHD2 del/del adipocytes show faster fatty acid uptake

A-B Oil Red O staining of cultured untreated pre-adipocytes and differentiated adipocytes (untreated: n(del(+) = 41/4, n(del/del) = 36/4); differentiated: n(del/+) = 84/6, n(del/del) = 106/8).

C-E Analysis of LD size in EHD2 del/del and EHD2 del/+ adipocytes by staining with BODIPY (untreated: n(del(+) = 74/3, n(del/del) = 60/3); differentiated: n(del/+) = 132/3, n(del/del) = 95/3). 3D reconstruction of EHD2 del/del differentiated adipocyte. Green – LDs, blue – nucleus.

F Cultivated EHD2 cKO flox/wt or flox/flox adipocytes were transfected with Cre recombinase-EGFP to induce EHD2 deletion and differentiated for 5 days, lipid droplets were stained with Nile Red for analysing (n(flox/wt) = 74/2, n(flox/flox) = 82/2).

G Pre-adipocytes were treated with either differentiation medium containing delipidated FBS or without glucose and BODIPY staining illustrating LDs.

H-I Fatty acid uptake assay in differentiated EHD2 del/+ and EHD2 del/del adipocytes. Dodecanoic acid-BODIPY uptake was measured after 5, 10, 20, 30 or 60 min, and R1 population indicates positively stained cells (illustrated in red in graphs H, I). R2 populations (blue) correspond to higher BODIPY staining intensity in cells and represent adipocytes with increased amount of dodecanoic acid taken up (shown in blue in graphs H, I).

J-M Overview of fatty acid uptake (percent cell numbers (J), normalization of EHD2 del/del R2 population relative to EHD2 del/+ R2 (K), time scale (L); J-L, n(del/+) = 6/3 experiments, n(del/del) = 8/3 experiments). Example images of differentiated adipocytes treated with dodecanoic acid for 60 min (M, scale bar 40 µm).
Column bar graphs and line graphs illustrate mean +/- SE, t-test or Mann Withney U test were used to calculate significance, * $P<0.05$; *** $P<0.0001$. See also Fig. S3.

680

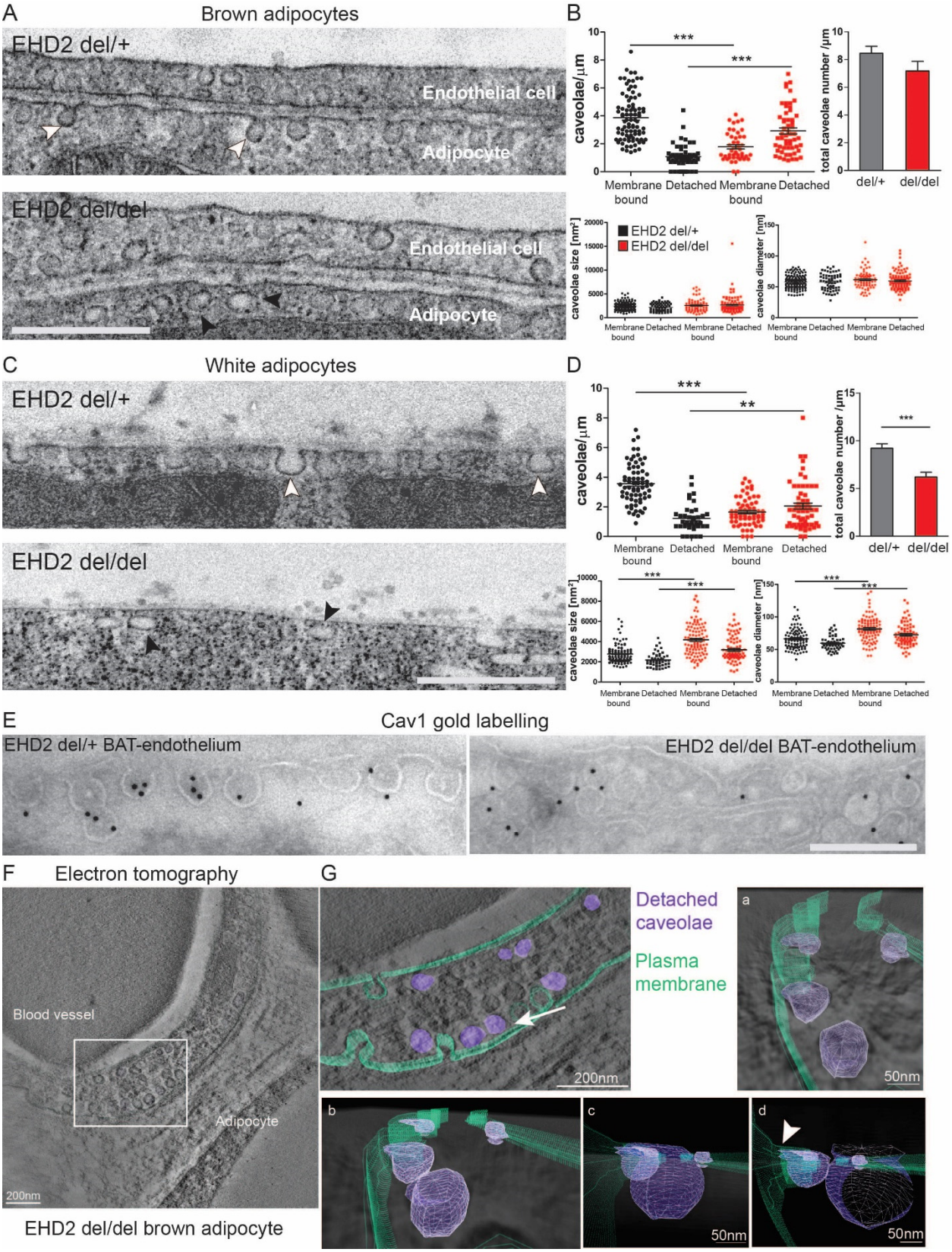

681

682 **Fig. 4: Loss of EHD2 resulted in detached caveolae *in vivo***

683 **A-B** Representative EM images of BAT from EHD2 del/+ and del/del mice and systematic analysis (caveolae
684 number: n(del/+) = 140/3, n(del/del) = 100/3; caveolae size and diameter: n(del/+) = 201/3, n(del/del) =
685 171/3). Scale bar 500 nm.

686 **C-D** EM images of EHD2 del/+ and del/del WAT (caveolae number: n(del/+) = 108/3, n(del/del) = 124/3;
687 caveolae size and diameter: n(del/+) = 151/3, n(del/del) = 185/3). Scale bar 500 nm.

688 **E** Representative image for EM gold immunolabeling against Cav1. Control labeling did not reveal specific
689 staining. Scale bar 200 nm.

690 **F-G** Electron tomogram of a 150 nm EHD2 del/del BAT section (F). The 3D model contains the plasma
691 membrane (G, green) and the detached caveolae (violet). Detachment of caveolae was observed by
692 changing the viewing angle (white arrow indicates the direction). Closer inspection of cell membrane and
693 caveolae clearly showed displacement of caveolae from the membrane. The 3D model also revealed
694 attachment of caveolae to the membrane (arrow head).

695 Graphs illustrate each replicate with mean +/- SE, t-test or Mann Withney U test were used to calculate
696 significance, ** $P<0.001$; *** $P<0.0001$. See also Movie S1.

697

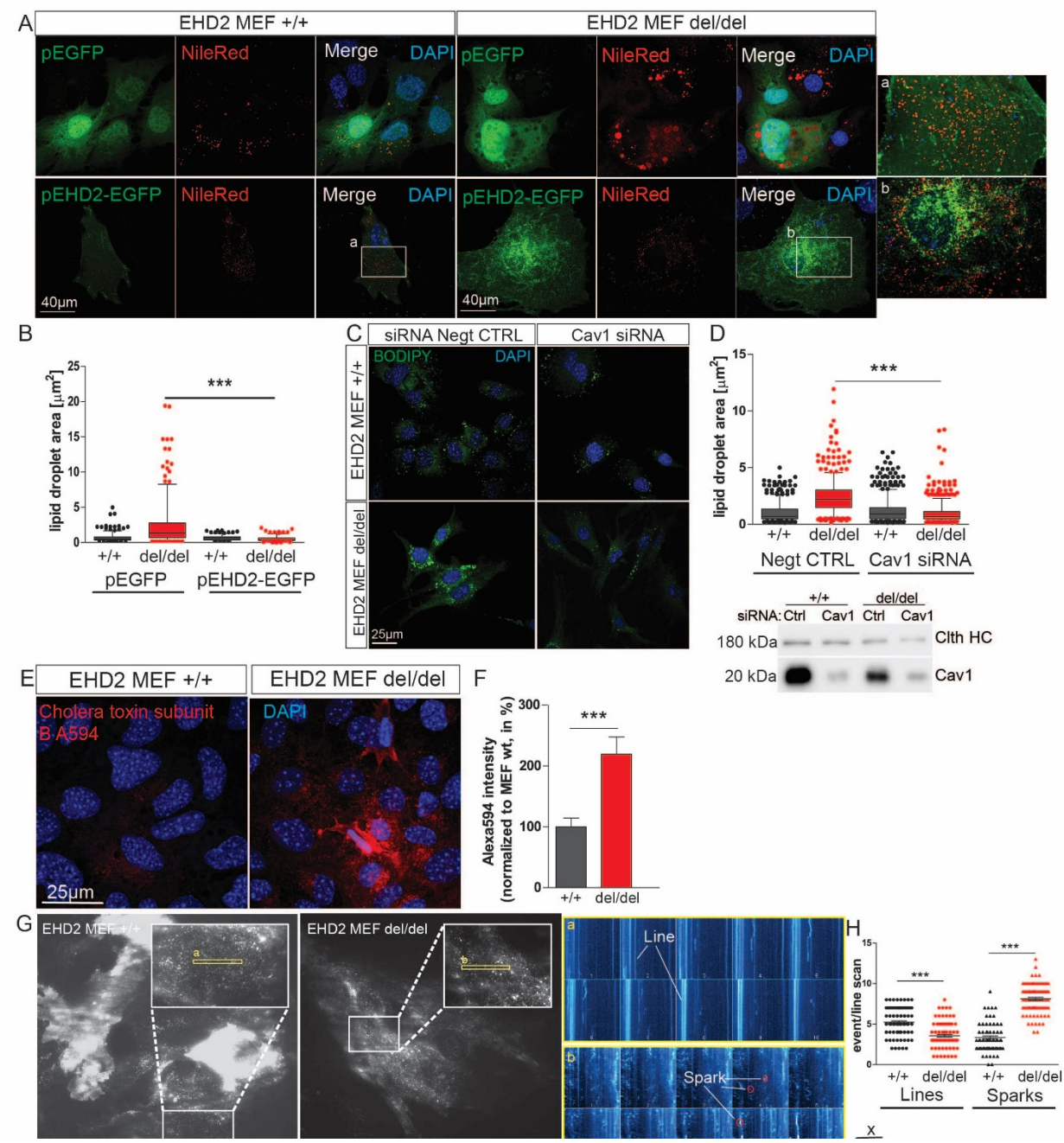

Fig. 5: Enhanced caveolar mobility in cells lacking EHD2

A-B EHD2 +/+ and del/del MEFS were transfected with either pEGFP or pEHD2-EGFP, incubated for 48 h and afterwards treated for 6 h with oleic acid and Nile Red staining was performed to determine LDs (pEGFP: n(+/+) = 309/3, n(del/del) = 310/3; pEHD2-EGFP: n(+/+) = 218/4, n(del/del) = 184/4).

C-D EHD2 del/del MEFs were treated with Cav1 siRNA and lipid droplets were stained with BODIPY (negative control: n(+/+) = 504/3, n(del/del) = 530/3; Cav1 siRNA: n(+/+) = 521/3, n(del/del) = 558/3); Clth HC - clathrin heavy chain.

E-F EHD2 MEFs were treated with Cholera toxin subunit B Alexa594 uptake in EHD2 +/+ and del/del MEFs after 30 min (F, n(+/+) = 40/5, n(del/del) = 40/6).

G-H TIRF live-imaging of EHD2 +/+ and del/del MEFs expressing pCav1-EGFP**.** Line scan analysis of the recorded Cav1 intensities revealed for fixed, non-moving caveolae lines and for fast moving caveolae

single sparks (as illustrated in a and b, n(+/+) = 90/3; n(del/del) = 92/3; each replicate is represented with mean +/- SE).
Box plots indicate maximal to minimum value with median, column bar graphs show mean + SE, t-test or Mann Withney U test were used to calculate significance, *** P<0.0001. See also Fig. S4 and Movie S2-4.

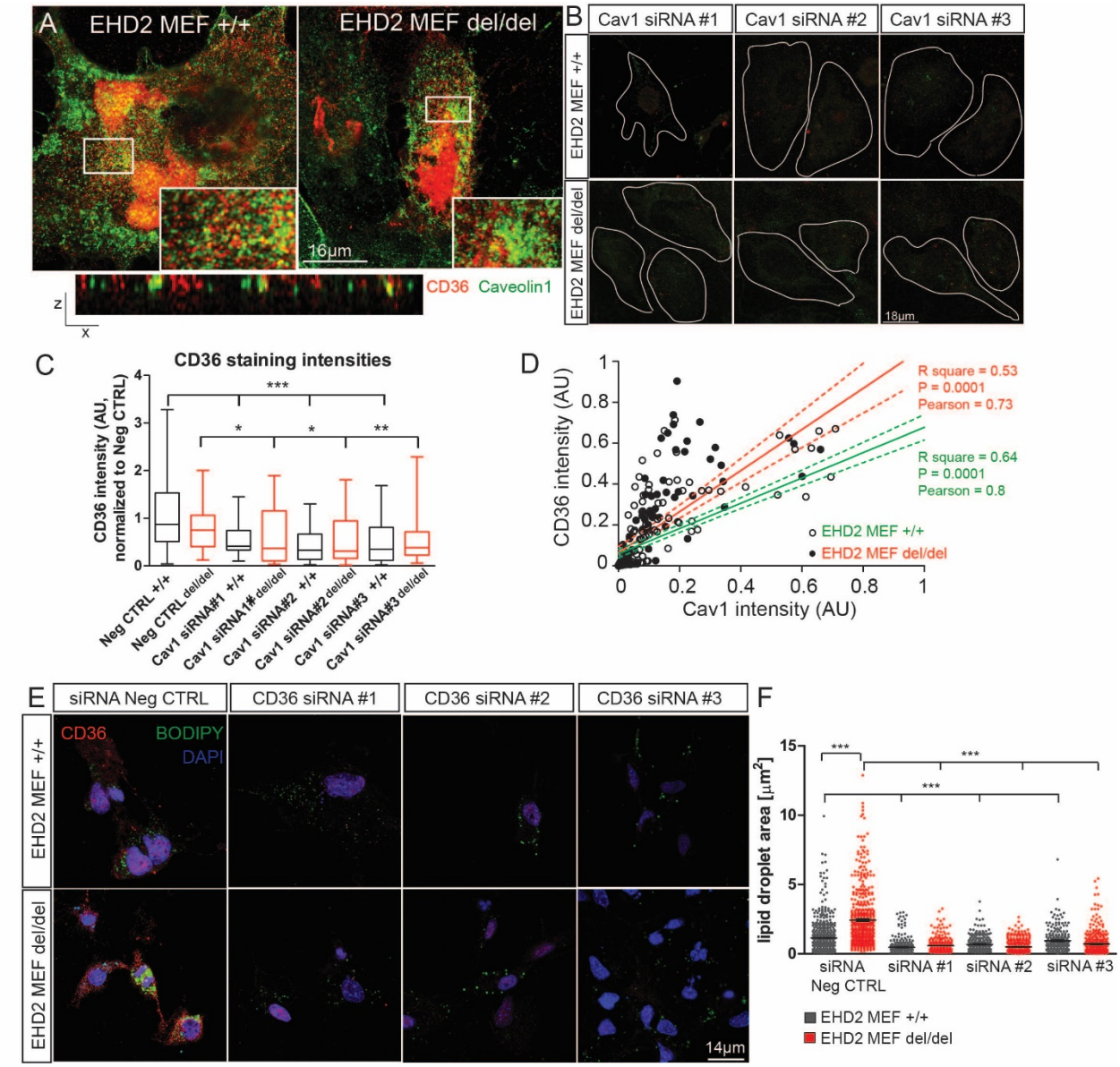

Fig. 6 Fatty acid translocase CD36 is involved in EHD2-mediated fatty acid uptake

A CD36 localization was investigated by antibody staining in EHD2 +/+ and del/del MEFs. Partial co-localization of CD36 and Cav1 was observed by confocal airyscan z-stack imaging.

B Example images for CD36 and Cav1 staining after Cav1 siRNA treatment in EHD2 +/+ and del/del MEFs (cells are indicated by white surrounding lines, compare to staining in A).

C Fluorescence intensity measurement of Cy3-Rabbit antibody after Rabbit-CD36 live staining in Cav1 siRNA treated MEFs (negative control: n(+/+) = 584/6, n(del/del) = 475/6; Cav1 siRNA#1: n(+/+) = 341/3, n(del/del) = 249/3; Cav1 siRNA#2: n(+/+) = 412/3, n(del/del) = 468/3; Cav1 siRNA#3: n(+/+) = 251/3, n(del/del) = 368/3; box plots indicate median with whiskers from maximal to minimum value, siRNA negative control was compared to Cav1 siRNA for statistical analysis).

D Correlation of Cav1 and CD36 staining intensities in EHD2 +/+ and del/del MEFs (n(+/+) = 150/4, n(del/del) = 120/4; Pearson correlation; graph shows each replicate and related linear regression including 95% confidence interval).

728 **E-F** LD size after CD36 siRNA knockdown in EHD2 +/+ and del/del MEFs (D, negative control: n(+/+) =
729 584/6, n(del/del) = 475/6; CD36 siRNA#1: n(+/+) = 341/3, n(del/del) = 249/3; CD36 siRNA#2: n(+/+) =
730 412/3, n(del/del) = 468/3; CD36 siRNA#3: n(+/+) = 251/3, n(del/del) = 368/3; graph illustrates each
731 replicate with mean +/- SE, 2-way ANOVA test were used to calculate significance between siRNA negative
732 CTRL and siRNA, t-test was used between +/+ and del/del data).
733 *P<0.05, **P<0.001, ***P<0.0001. See also Fig. S5.

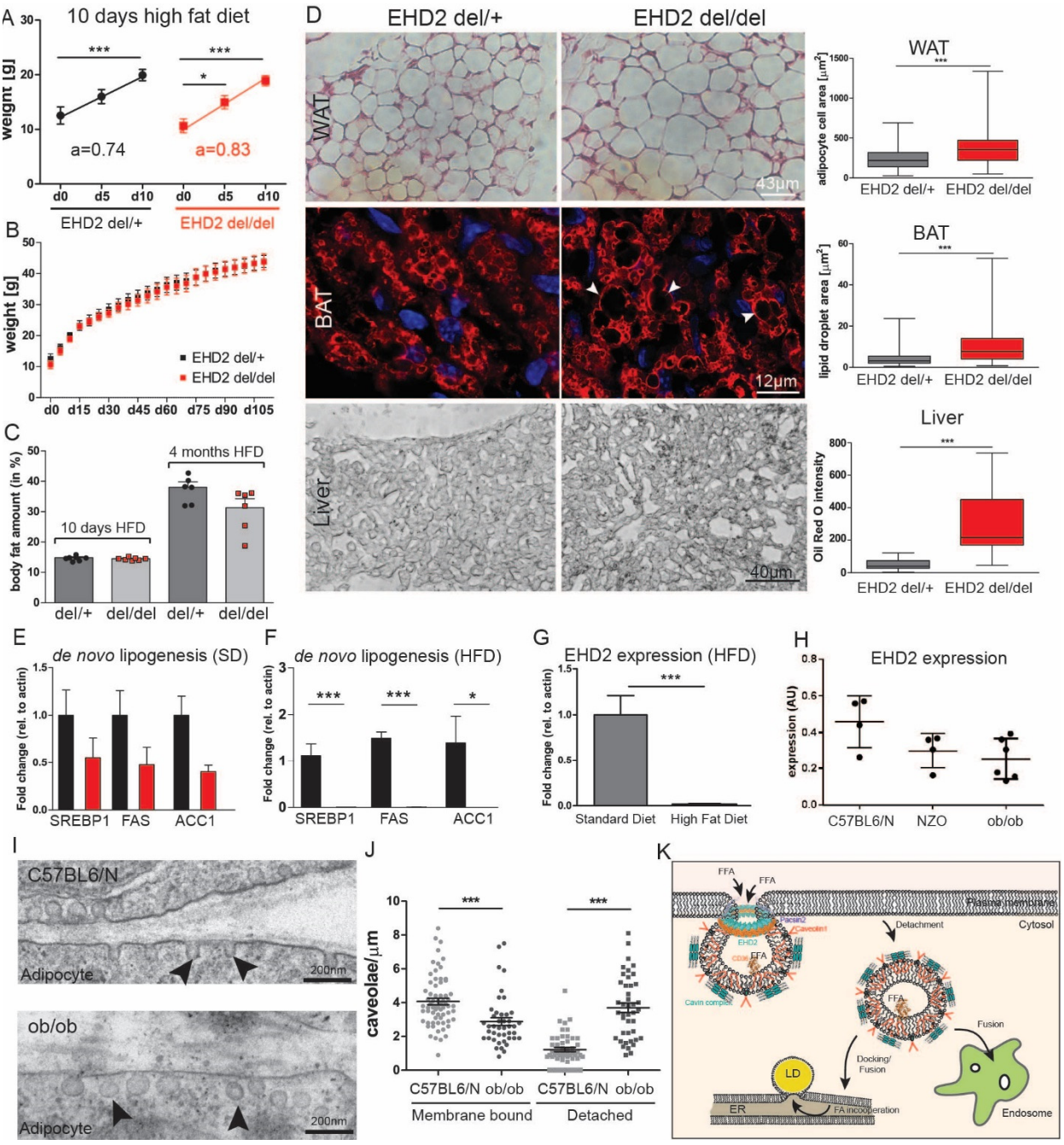

Fig. 7: Decreased EHD2 expression in diet induced obesity and genetic obesity mouse models

A-B EHD2 del/+ and EHD2 del/del mice were fed with a high fat diet (60% kcal fat) for 10 days (A) or 4 months (B) and body weight was measured every 5 days (A, n(day 0-10) = 12; B, n(day 15-110) = 6).

C Body composition analysis after 10 days or 4 months of high fat diet (n(10 days high fat diet) = 7; n(4 months of high fat diet) = 6).

D After 10 days high fat feeding, adipocyte cell sizes were analyzed in EHD2 del/+ and EHD2 del/del WAT paraffin sections (n(del/+) = 317/2; n(del/del) = 337/2). BAT cryostat sections were stained against Perilipin1 (red – Perilipin1, blue – DAPI; n(del/+) = 263/2; n(del/del) = 236/2). Oil Red O staining of liver

744 sections obtained from EHD2 del/+ and EHD2 del/del mice fed for 10 days with high fat diet (n(del/+) =
745 28/2; n(del/del) = 29/2).
746 **E-F** Expression levels of genes involved in *de novo* lipogenesis in EHD2 del/del and del/+ WAT following
747 standard diet (SD, E) or high fat diet (HFD, F; n(SD) = 8-12/4; HFD, n(del/+) = 8/3, n(del/del) = 6/3).
748 **G** EHD2 expression in white adipocytes of EHD2 del/+ mice fed with high fat diet (HFD) compared to EHD2
749 del/+ mice under standard diet (n = 5).
750 **H** EHD2 expression level was analyzed in fat tissue of ob/ob or NZO mouse models compared to C57BL6/N
751 mice (n = 5, graph illustrates mean +/- SE).
752 **I-J** Investigation of caveolae by EM imaging (n(ob/ob mice) = 85/2; n(C57BL6/N) = 117/2; graph illustrates
753 mean +/- SE).
754 **K** The model illustrates the EHD2-caveolae dependent fatty acid uptake. CD36 localizes within caveolae,
755 consequently, CD36 can bind and transfer free fatty acids (FFA) through the plasma membrane (PDB:
756 5LGD, (Hsieh *et al.*, 2016)). After loss of EHD2, the enhanced mobility and detachment of caveolae results
757 in an increased fatty acid uptake either via direct fusion or docking to the ER or via the endosomal pathway
758 (FFA - free fatty acid, ER – endoplasmic reticulum, LD – lipid droplet).
759 Box plots indicate median with whiskers from maximal to minimum value, column bar and line graphs
760 show mean +/- SE, normal distributed groups were analyzed by t-test, not normal distributed values with
761 Mann Withney U test, * P<0.05, *** P<0.0001. See also Fig. S5-6.
762

Material and Methods

EHD2 delta E3 mouse strain generation. The EHD2 targeting construct was generated by insertion of two lox P sequences flanking exon 3 of EHD2 genomic DNA by homologous recombination in *E.coli* as previously described (Liu *et al.*, 2003). A pGK Neomycin and a diphtheria toxin A (DTA) cassette was included to enrich for correctly targeted ES cells. Electroporation of the linearized targeting vector in R1 ES cells was performed. For southern blot analysis, genomic DNA from G418-resistant ES clones was digested with BamHI and EcoRV and probed with PCR fragments to confirm correct integration (BamHI-Probe: Primer-FWD: 5- CACGCGGTCCAGCTGGCTTCA-3', Primer-REV: 5'- GTG GCT GAA GAG TCT ATG CAC TTC GAG-3'; EcoRV-Probe: Primer-FWD: 5'- CAG GCC CCA CGC TTC AGG ATT TTA ACT G-3', Primer-REV: 5'- GCC TTG TTG AGT ACC ACG CGG ATC-3'). Correctly targeted ES clones were injected into C57Bl6 blastocyst. The offspring was genotyped by PCR. Mice carrying a loxP-flanked Exon 3 of EHD2 gene were mated to Cre deleter mice to generate EHD2 mutant (del/del) mice. After backcrossing the EHD2 del/del mice with C57BL6/N (Charles River, between 20-30 weeks, male) for 6 generations only male EHD2 del/del or EHD2 del/+ (as control) mice were used and littermates were randomly assigned to experimental groups. All animals were handled accordingly to governmental animal welfare guidelines and were housed under standard conditions. If not otherwise indicated mice were sacrificed at an age of 20-30 weeks (for cell culture preparation) or 40-50 weeks (organ dissection).

Obesity Mouse Models. Male NZO/HIBomDife (German Institute of Human Nutrition, Nuthetal, Germany), C57BL/6J (Charles River Laboratories, Sulzfeld, Germany) and B6.V-Lepob/ob/JBomTac (B6-ob/ob) mice (Charles River Laboratories, Calco, Italy) were housed under standard conditions (conventional germ status, 22 °C with 12 hour /dark cycling). NZO and C57BL/6J mice were fed were fed standard chow diet (Ssniff, Soest). Starting at 5 weeks of age B6-ob/ob received carbohydrate free diet (Kluth *et al.*, 2015). Mice were sacrificed at an age of 20-22 weeks.

High Fat Diet. To investigate *in vivo* fat uptake the EHD2 delta E3 mice were fed with a high fat diet (OpenSource Diets, D12492, 60% kcal) according to our animal application. In total, 16 EHD2 del/+ and 16 EHD2 del/del mice were investigated whereby only male, backcrossed animals were used (>F5 generation, backcrossing with C57BL6/N). The high fat diet was immediately applied after weaning for maximal 16 weeks. The body weight was monitored every 5 days. 7 mice/genotype were fed for 10 days with high fat diet and afterwards the body composition (BRUKER MiniSpec LF90II) was measured.

Mouse embryonic fibroblast isolation and immortalization. All animals were handled accordingly to governmental animal welfare guidelines. MEFs were obtained from E14.5 EHD2 +/+ or del/del embryos. Therefore female, pregnant EHD2 del/+ were sacrificed by cervical dislocation, the embryos were

795 dissected and removed from the yolk sac in sterile, cold PBS. For genotyping, a small piece of each mouse
796 embryo tail was harvested followed by complete dissection of the whole embryo. Afterwards, the embryo
797 pieces were treated with 0.25% trypsin/EDTA (Sigma) over night at 4 °C. After aspiration of the trypsin
798 solution, 10 ml culture medium (DMEM/10%FBS/5% penicillin/streptomycin) was added and tissue pieces
799 were break up by pipetting. The cell suspension was transferred in 75 cm^2 culture flask for cultivation at
800 37 °C and 5% CO_2. Immortalization of isolated primary MEFs was assured by frequently splitting. From
801 passage 15 an increased growth rate was observed suggesting immortalized MEFs. For all experiments
802 MEFs between passage 12 and 32 was used. For LD growth, MEFs were either treated with 10 µg/ml
803 insulin, 2.5 mM dexamethasone, 50 mM IBMX and 25 mM rosiglitazone diluted in culture medium
804 (differentiation medium) or 0.016 M oleic acid and 10 µg/ml insulin diluted in DMEM.
805 **Primary adipocyte cell culture.** Male EHD2 del/+ and EHD2 del/del mice or EHD2 cKO flox/wt or flox/flox
806 were sacrificed by cervical dislocation and gonadal WAT was removed. Adipocytes and stromal vascular
807 fraction (SVF) were isolated after washing the tissue in sterile PBS and digestion by collagenase type II
808 (Sigma C6885). Mature adipocytes floating in the upper phase were transferred in a new flask and diluted
809 with culture medium (DMEM/10%FBS/5% penicillin/streptomycin), SVF was obtained after 5 min
810 centrifugation at 1,000 rpm. After complete tissue break up the adipocyte cell suspension was passed
811 through a 270 µm cell strainer and the cells were plated in 75 cm^2 culture flask at 37 °C and 5% CO_2
812 whereby pre-adipocytes adhere to the flask and mature adipocytes float in the medium. SVF suspension
813 was cleaned by passing through 70 µm cell strainer. The following day the culture medium was exchanged
814 to remove dead or non-adherent cells. After 5 days, both pre-adipocytes and SVF were split by 0.25%
815 trypsin/EDTA solution and merged for further cultivation. Differentiation to mature adipocytes was
816 induced by 10 µg/ml insulin, 2.5 mM dexamethasone, 50 mM IBMX and 25 mM rosiglitazone diluted in
817 culture medium. If not otherwise mentioned the primary pre-adipocytes were incubated for 5 days with
818 differentiation medium and medium was changed after 2 days. Delipidation of FBS was carried out as
819 described by (Cham and Knowles, 1976). EHD2 cKO adipocytes were transfected with Cre recombinase-
820 EGFP by using adeno-associated virus particles 8 (AAV8) produced from pAAV.CMV.HI.eGFP-
821 Cre.WPRE.SV40 (addgene, #105545). The adipocyte cell culture was transfected and differentiated for 5
822 days.
823 **Oil Red O staining.** LDs in tissue sections or cultivated adipocytes and MEFs were stained with Oil Red O
824 as published by (Mehlem *et al.*, 2013). Briefly, freshly dissected liver of muscle pieces were frozen in liquid
825 nitrogen, embedded in TissueTek and 10 µm cryostat sections (Leica) were prepared. After fixation with
826 4% para-formaldehyde (PFA, Merck) freshly prepared Oil Red O staining solution was applied for 10 min.

827 The sections were washed with PBS and embedded in ImmoMount (Invitrogen). Cultivated cells were
828 fixed, treated with 60% isopropanol (Merck) for 2 min and then incubated with Oil Red O staining solution
829 for 5 min. After washing with water until complete removal of Oil Red O the stained cells or sections were
830 analyzed by Zeiss Axiovert microscope (20x Zeiss objective). Staining intensity was measured with ImageJ.
831 **Histology.** EHD2 del/+ and EHD2 del/del mice were anesthetized with 2% ketamine/10%rompun, perfused
832 first by 30 ml PBS and next by 50 ml 4% PFA and tissues were dissected. After 24 h of fixation in 4% PFA,
833 tissues were dehydrated in 3 steps (each 24h) from 70-100% EtOH and afterwards incubated in xylol
834 (Merck) for 48 h. Next, the tissues were embedding in liquid paraffin at ca. 65°C and cooled down on ice.
835 4 µm paraffin sections were obtained, de-paraffinized and hydrated and Masson Trichrome staining (Kit,
836 Sigma) was applied. Briefly, sections were stained with Bouin solution for 15 min at 60°C, followed by
837 Haematoxylin Gill No. 2 staining for 5 min and incubation in Biebrich-Scarlet-Acid Fuchsin for 5 min. Next,
838 the tissue sections were treated with Phosphotungstic/Phosphomolybdic Acid Solution and Aniline Blue
839 solution both for 5 min, and acetic acid treatment (1%) for 2 min. After extensive washing the sections
840 were dehydrated, incubated in xylol and embedded with Roti Histo Kit (Carl Roth). Images were obtained
841 at Zeiss Axiovert100 microscope.
842 **Immunohistostaining of cryostat sections.** Perfused and fixated EHD2 del/+ and EHD2 del/del mice (as
843 described before) were dissected and the investigated tissue pieces were further fixed for 1-4 h in 4% PFA,
844 transferred to 15% sucrose (in PBS, Merck) for 4 h and finally incubated overnight in 30% sucrose. After
845 embedding in TissueTek, the tissue is frozen at -80 °C. 5-15 µm sections were obtained in a cryostat at -
846 20 - -30 °C and stored at -20 °C. For immunostainings, the cryostat sections were incubated with blocking
847 buffer (1% donkey serum/1% TritonX100/PBS) for 1 h at room temperature, and treated overnight at 4°C
848 with the first antibody diluted in blocking buffer. After washing with PBS/1%Tween, the secondary
849 antibody was applied for 2 h at room temperature. After completion of the staining, the sections were
850 washed carefully and embedded in ImmoMount. The stained sections were analyzed with Zeiss LSM700
851 microscope provided with Zeiss objectives 5, 10, 20, 40 and 63x. The obtained images were further
852 investigated by ZEN software and ImageJ/Fij.
853 **Immunocytostaining and LD staining of cultivated cells.** Adipocytes or MEFs were seeded on fibronectin
854 (Sigma) coated glass dishes (12 mm diameter, Thermo Fisher) in cell concentration ranging from 20.000-
855 40.000 cells/well depending on treatment and experiment. Before the staining, cells were washed with
856 PBS, treated with 4% PFA for 10 min and blocking buffer (1%donkey serum/1% TritonX100/PBS) was
857 applied for 20 min. The first antibody was diluted in blocking buffer and the cells were incubated with 200
858 µl antibody solution for 1 h. After washing with PBS the secondary antibody and DAPI (1:1000, Sigma) was

applied for 1 h. For LD staining, BODIPY (Invitrogen) or Nile Red (Sigma) was diluted to 1:500 in cold PBS and after washing and fixation of the cells, the BODIPY or Nile Red staining solution and DAPI (1:1000) was applied for 30 min. The stained cells were washed and the glass dishes were placed on conventional microscope slides and embedded in ImmoMount. The antibody staining was investigated by Zeiss LSM700 or Zeiss LSM880 microscope and images were analyzed in detail with ImageJ/Fij.

Transfection and siRNA knockdown. Cultivated MEFs were transfected with the following plasmids pEHD2-EGFP, pCav1-EGFP or pEGFP by lipofectamine 3000 accordingly to the manufacture's protocol. Transfected cells were incubated for 48 h and afterwards the treated cells were analyzed by confocal microscopy or TIRF. siRNA knockdown of CD36 or Cav1 was performed in freshly split MEFs by electroporation with the GenePulser XCell (Biorad). Briefly, MEFs were split as described before and the obtained cell pellet was resuspended in OptiMEM (Gibco). After cell counting, the MEF cell suspension was diluted to $1.5x10^6$ cells/ml and 300 µl were transferred into electroporation cuvettes (2 mm, Biorad). CD36 or Cav1 stealth siRNA and siRNA negative control (medium GC content) was added to a final concentration of 200 nM. After carful mixing, the cuvettes were placed into the electroporation device and the pulse (160 µOHM, 500 µF, ∞ resistance) was applied. The electroporated cells were cultivated in DMEM/10%FBS for 48 h before the experiments were started. Successful siRNA knockdown was monitored by CD36 antibody staining.

Cholera toxin subunit B uptake assay. MEFs were plated on fibronectin coated glass dishes and cultivated for 48 h. The cholera toxin uptake assay was performed as described by (Sotgia *et al.*, 2002). Briefly, after washing twice with cold PBS cholera toxin subunit B labelled with Alexa594 was applied to the cells. The treated MEFs were incubated for 30 min in the dark on ice. Afterwards the cells were washed twice with PBS and incubated for 30 min with cultivation medium at 37 °C. After fixation with 4% PFA, DAPI staining solution was added for 10 min. Before embedding in ImmoMount, the cells were washed PBS. Cholera toxin uptake was analyzed with a Zeiss LSM700 microscope with a 63x Zeiss objective. The Alexa594 staining intensity was measured by ImageJ. For each experiment 10 different cells were examined.

TIRF live imaging of caveolae movement. MEFs transfected with pCav1-EGFP were incubated for 48 h on fibronectin coated cover slips (25 mm diameter). Samples were mounted in Attofluor Cell Chamber (Thermo) in a physiological buffer (130 mM NaCl, 4 mM KCl, 1.25 mM NaH_2PO_4-H_2O, 25 mM $NaHCO_3$, 10 mM glucose, 2 mM $CaCl_2$, 1 mM $MgCl_2$, pH 7.3, 305-315 mOsm/kg).

TIRF imaging was performed on an inverted Microscope (Nikon Eclipse Ti) equipped with a 488 laser (Toptica), an dicroic mirror (AHF, zt405/488/561/640 rpc), a 60x TIRF objective (Nikon, Apo TIRF NA 1.49), an appropriate emission filter (AHF, 400-410/488/561/631-640) and a sCMOS camera (mNeo, Andor). All

components were operated by open-source ImageJ-based micromanager software. All experiments were performed at 37 °C. To investigate the movement of single caveolae transfected cells were selected in which regions of individual Cav1 spots were observed (ROIs illustrated in Fig. 4J, enhanced images). Recordings were obtained with the following imaging settings: image size 1776x1760 pixel, 1x1 binning, 500 frames, 200 ms exposure time/frame. For data analysis only the first 150 frames were investigated. After cropping to the specific ROI, kymograph analysis of several positions within the ROIs were carried out using the Reslice function of ImageJ/Fij. Carefully investigation of the kymographs revealed a single, straight line for fixed, not moving caveolae and sparks or short lines for fast moving caveolae.

Transmission Electron microscopy (TEM). Mice were fixed by perfusion with 4% (w/v) formaldehyde in 0.1 M phosphate buffer and tissues were dissected to 1-2 mm^3 cubes. For morphological analysis, tissue blocs were postfixed in phosphate buffered 2.5% (v/v) glutaraldehyde. Samples were treated with 1% (v/v) osmium tetroxide, dehydrated in a graded series of ethanol and embedded in the PolyBed® 812 resin (Polysciences Europe GmbH). Ultrathin sections (60-80 nm) were cut (Leica microsystems) and stained with uranyl acetate and lead citrate before image acquisition. For immuno-labeling, samples were fixed by perfusion as described above, but postfixed in phosphate buffered 4% (w/v) formaldehyde with 0.5% (v/v) glutaraldehyde for 1 hour. Samples were further processed as described in Slot and Geuze (Nature protocols, 2007). Briefly, samples were infiltrated with 2.3 M sucrose, frozen in liquid nitrogen and sectioned at cryo temperatures. Sections were blocked and washed in PBS supplemented with 1% BSA and 0.1% glycine. Labeling was performed with an anti-caveolin-1 antibody 1:500 (abcam #2910) and 12 nm colloidal gold (Dianova). Sections were contrasted with 3% tungstosilicic acid hydrate (w/v) in 2.8% polyvinyl alcohol (w/v) (Kärgel *et al.*, 1996). Samples were examined at 80 kV with a Zeiss EM 910 electron microscope (Zeiss). Acquisition was done with a Quemesa CDD camera and the iTEM software (Emsis GmbH).

Electron tomography (ET). To obtain electron tomograms 250 nm slices of EHD2 del/del BAT were prepared of samples embedded in resin and treated as described for TEM. The samples were tilted from 60 to -60° in 2° steps and examined at 120 kV with a FEI Talos electron microscope. FEI tomography software was used for acquisition of tomograms, detailed analysis and reconstruction was done with Inspect3D, Amira (both obtained from FEI) and IMOD (University of Colorado, USA).

***In situ* hybridization.** Digoxigenin-labeled riboprobes were generated using a DIG-RNA labeling kit (Roche). In situ hybridizations were performed on 14 µm cryosections prepared from E18.5 wt embryos as previously described (Wilkinson, 1993). To generate an Ehd2 specific in situ probe, a 400 bp fragment was amplified from wildtype cDNA using PCR and primer listed below. The PCR product was cloned into

pGEM-Teasy (Promega). T7 and sp6 polymerases were used to generate Ehd2-sense and antisense probes, respectively.

EDH2_ISH_FWD: 5'-CAGGTCCTGGAGAGCATCAGC-3'

EDH2_ISH_REV: 5'- GAGGTCCTGTTCCTCCAGCTCG-3'

Western Blot. EHD2 protein level in different tissues was examined by Western Blot. Therefore EHD2 +/+, EHD2 del/+ and EHD2 del/del mice were sacrificed by cervical dislocation and organs were dissected and snap frozen in liquid nitrogen. After homogenization of the tissue in 1x RIPA buffer (Abcam) with a glass homogenizer, the tissue lysate was incubated for 1 h on ice followed by 15 min centrifugation at 15,000 rpm. Supernatant was transferred in a fresh tube and protein concentration was measured by NanoDrop. At least 10 µg protein/lane was applied to 4-12% SDS-PAGE NuPage (Invitrogen) and SDS-PAGE was performed accordingly to the manufacture's protocol. Afterwards, proteins were blotted on nitrocellulose membrane (Amersham) at 80 V for 1 h, followed by blocking of the membranes with 5% milk powder (in TBST, 150 mM NaCl, 20 mM Tris-HCl, pH 7.5, 0.1% Tween20) for 2 h at room temperature. To detect EHD2 protein level rabbit-anti-EHD2 (1:2,000) was applied over night at 4 °C. After washing with TBST the secondary antibody goat-anti-rabbit-HRP was added to the membrane for 2 h at room temperature. Detection of EHD2 bands results from ECL detection solution and intensities were obtained by ChemiDoc XRS (Biorad). Please see key resources table for all antibodies used in this study.

Blood plasma analysis. To measure distinct blood plasma parameter related to metabolic changes like adiponectin, insulin or free fatty acids blood was taken from EHD2 del/+ and EHD2 del/del mice immediately after cervical dislocation. All blood samples were taken at 10.00 am. Briefly, mice were opened and the thorax was partly removed to get access to the left heart ventricle, a cannula was inserted and blood samples were taken. After short centrifugation at high speed, the plasma fraction was transferred to a fresh tube and snap frozen in liquid nitrogen. The following assays were used to measure the described blood plasma markers: Plasma insulin levels were measured by Mouse Ultrasensitive Insulin ELISA (80-INSMSU-E10, Alpco). Plasma adiponectin and leptin levels were measured by Mouse Adiponectin/Acrp30 (DY1119) and Mouse/Rat Leptin (MOB00) ELISA kits (R&D Systems). Plasma lipids were quantified with commercially available kits: cholesterol (Cholesterol liquicolour colorimetric assay, Human, Wiesbaden, Germany), triglycerides/glycerol (Triglyceride/Glycerol Calorimetric Assay, Sigma) and non-esterified fatty acids (Wako Chemicals). All measurements were done according to manufacturers' recommendations.

Fatty acid uptake assay. EHD2 del/+ and EHD2 del/del pre-adipocytes were seeded in 6-well plates (100.000 cells/well) and differentiated in mature adipocytes as described above. The fatty acid uptake

assay was performed as described elsewhere (Dubikovskaya *et al.*, 2014). Briefly, after 5 days of differentiation, adipocytes were starved for 1 h with serum-free DMEM. Next, 2 µM dodecanoic acid (FA12) labelled with BODIPY (Molecular probes #D3822) diluted in serum-free DMEM + 10 µg/ml insulin was added to the adipocytes and incubated for 5, 10, 20, 30 and 60 min at 37 °C. After washing twice with ice-cold PBS, 150 µl 0.25% trypsin/EDTA/PBS was applied to detach the cells. The adipocytes were treated with 500 µl ice-cold FACS buffer (HBSS/10%FBS/10 mM EDTA) and the cell solution was transferred to FACS tubes. Shortly before measurement, 1 µl/ml propidium iodide was added. FACS experiments were performed at LSR Fortessa 5Laser with the following parameters: FSH: A, H, W, Voltage 255; SSC: A, H, W, Voltage 203; A488: A, Voltage 198; PE: A, Voltage 341. For each FACS sample 30.000 cells were investigated. As negative control unstained EHD2 del/+ and EHD2 del/del adipocytes were examined at first and the obtained BODIPY intensity values were used as a reference for unstained cells. To exclude adipocytes which did not show any positive fatty acid uptake, all unstained cells were removed resulting in an only positive stained population (R1, illustrated in red in Fig. 3G and H). Within this R1 population adipocytes with strongly increased BODIPY intensity values were gated to population R2 (blue, Fig. 3G, H). Detailed analysis/gating and statistics was done by using FlyingSoftware2.5.1 (Perttu Terho, Cell Imaging Core, Turku Center for Biotechnology). For each experiment 15.000 cells were analyzed and gated to the unstained, R1 or R2 population. Next, the percentage of the cells gated to the populations were calculated for every time point and illustrated in the bar graph (Fig. 3I). R2 population was investigated in more detail by normalization to the R2 cell number of EHD2 del/+ adipocytes (Fig. 3J).

Glucose uptake assay. Glucose uptake of EHD2 del/+ and EHD2 del/del adipocytes was measured as described by BioVison (2-NBDG Glucose uptake assay). Briefly, adipocytes were treated as described for fatty acid uptake assay. However, after starvation 200 µM 2-NBDG (2-deoxy-2-[(7-nitro-2,1,3-benzoxadiazol-4-yl) amino]-D-glucose, molecular probes #N13195) diluted in serum-free DMEM + 10 µg/ml insulin was applied to the cells followed by incubation times from 5-60 min. Staining analysis was done as mentioned for fatty acid uptake with the same FACS parameters and gating procedure whereby only one positive stained cell population was examined (R1, illustrated in Fig. S3A).

Gene expression analysis. EHD2 del/+ and EHD2 del/del adipocytes were differentiated for 5 days, washed twice with ice-cold PBS and RNA was isolated accordingly to the Qiagen protocol (RNeasy Mini Kit, Qiagen). SuperscriptIII First Strand Synthesis Kit (Invitrogen #18080051) was used to obtain corresponding cDNA, which then was used for real-time PCR. Gene expression levels were analyzed by GoTaq q-PCR (Promega, #A6001) Master Mix in Fast real time PCR cycler (Applied Biosystems) accordingly to instructor's protocol. To measure the relative fold change of genes in EHD2 del/del adipocytes

compared to EHD2 del/+, the comparative real-time PCR method was applied whereby actin was used as reference gene. Please see key resource table for detailed primer description.

Total mRNA from murine gonadal adipose tissue (gWAT) was extracted with RNeasy Mini Kit (QIAGEN GmbH, Hilden) according to manufacturer's instructions. RNA was transcribed using the Moloney Murine Leukemia Virus Reverse Transcriptase (M-MLV RT, Promega) according to manufacturer's recommendations. Expression of mRNA was determined by quantitative real-time PCR on LightCycler 480 II/384 (Roche, Rotkreuz, Switzerland) using GoTaq Probe qPCR Master Mix (Promega, Madison, USA) applying TaqMan Gene Expression Assays. Target gene expression of was normalized to the mean expression of *Eef2*, *Ppia* and *Actb* in murine samples.

Gene	Description	TaqMan Assay
EHD2	EH-domain containing 2	Hs.PT.58.4969281
Ehd2	EH-domain containing 2	Self-designed
Actb	Actin, beta	Self-designed
Eef2	Eukaryotic translation elongation factor 2	Self-designed
Ppia	Peptidylprolyl isomerase A	Mm.PT.39a.2.gs

Actb

Left primer: TACGACCAGAGGCATACAG

Right primer: GCCAACCGTGAAAAGATGAC

Probe: TTGAGACCTTCAACACCCCAGCCA

***Eef2* (Integrated DNA Technologies)**

Left primer: CACAATCAAATCCACCGCCA

Right primer: TGAGGTTGATGAGGAAGCCC

Probe: TAAGCAGAGCAAGGATGGCT

***Ehd2* (UPL, Roche)**

Left primer: CAGCTGGAGCACCACATCT

Right primer: TCATGTGCCATCAACAGCTC

UPL probe: #80

Lipid composition. The measurement of lipid amount and its composition in tissue samples or cells were performed by Lipotype GmbH (Dresden, Germany). For this, tissue samples were homogenized

accordingly to the supplied Lipotype protocol and diluted samples (1 mg/ml) were frozen and analyzed by Lipotype. MEF were split and the cell pellet was diluted in cold PBS to a final cell number of 30,000 cells/ml.

Type 2 Diabetes Knowledge Portal – *Ehd2* gene info. Ehd2 mutations in patients suffering from T2D were investigated via the T2D knowledge portal: Type 2 Diabetes Knowledge Portal. *EHD2*. type2diabetesgenetics.org (NIH Accelerating Medicines Partnership, 2014). 2018 May 16, http://www.type2diabetesgenetics.org/gene/geneInfo/EHD2, http://exac.broadinstitute.org/gene/ENSG00000024422

Statistical analysis. At first, a normality distribution test (Kolmogorov-Smirnov test) was carried out for all experimental values. If the data was normally distributed, Student t-Test (two-tailed P-value) was applied, otherwise Mann-Withney-Rank-Sum (two-tailed P-value) test was used to calculate the significant difference between two groups. Cav1 and CD36 staining intensities were correlated for EHD2 wt and KO MEFs (Fig. 6D) by using Pearson correlation. The correlation and the 95% confidence interval was calculated by Prism (GraphPad software). Two-way-Anova tests were used to investigate LD size after CD36 siRNA knockdown, whereby for EHD2 wt and KO MEFs each CD36 siRNA#1-3 treated cells were compared to nonsense siRNA (negative control, Fig. 6F). Box plots, if not otherwise indicated in the figure legends, always represents median with whiskers from minimum to maximum, column bar graphs and line graphs represent mean with mean standard error of the mean (SE). Statistical calculations were carried out by using Prism (GraphPad software). Distribution of LD sizes represented in histograms were also obtained by using Prism. For all experiments including the examination of mice or mouse tissue, n represents the number of mice which were used (Fig. 1, 2, 4, 7, S6, S7) and all analyzed cryo/paraffin sections or caveolae are also indicated (e.g.: n = 80 caveolae/3 mice). In cell culture experiments (Fig. 3, 5, 6, S3, S4, S5), n represents the number of observed events (e.g.: lipid droplet area, staining intensity) and the number of independently performed experiments (e.g.: n = 80 lipid droplets/3 independent

1035 experiments). The following P-values were used to indicate significant difference between two groups: *

1036 P<0.05; ** P<0.001; *** P<0.0001.

1037